

The hidden structure of innovation networks

Lorenzo Emer,^{1,2} Anna Gallo,^{3,4} Mattia Marzi,³ Andrea Mina,^{1,5} Tiziano Squartini,^{3,4,*} and Andrea Vandin^{1,6}

¹*Institute of Economics and L'EMbeDS, Scuola Superiore Sant'Anna,
P.zza Martiri della Libertà 33, 56127 Pisa (Italy)*

²*Department of Computer Science, University of Pisa, L.go Bruno Pontecorvo 3, 56126 Pisa (Italy)*

³*IMT School for Advanced Studies, P.zza San Francesco 19, 55100 Lucca (Italy)*

⁴*INdAM-GNAMPA Istituto Nazionale di Alta Matematica 'Francesco Severi', P.le Aldo Moro 5, 00185 Rome (Italy)*

⁵*Centre for Business Research, University of Cambridge,
Trumpington Street 11-12, CB2 1QA Cambridge (UK)*

⁶*DTU Technical University of Denmark, Anker Engelunds Vej 101, 2800 Kongens Lyngby (Denmark)*

(Dated: January 19, 2026)

Innovation emerges from complex collaboration patterns - among inventors, firms, or institutions. However, not much is known about the overall mesoscopic structure around which inventive activity self-organizes. Here, we tackle this problem by employing patent data to analyze both individual (*co-inventorship*) and organization (*co-ownership*) networks in three strategic domains (*artificial intelligence*, *biotechnology* and *semiconductors*). We characterize the mesoscale structure (in terms of clusters) of each domain by comparing two alternative methods: a standard baseline - modularity maximization - and one based on the minimization of the Bayesian Information Criterion, within the Stochastic Block Model and its degree-corrected variant. We find that, across sectors, inventor networks are denser and more clustered than organization ones - consistent with the presence of small recurrent teams embedded into broader institutional hierarchies - whereas organization networks have neater hierarchical role-based structures, with few bridging firms coordinating the most peripheral ones. We also find that the discovered meso-structures are connected to innovation output. In particular, Lorenz curves of forward citations show a pervasive inequality in technological influence: across sectors and methods, both inventor (especially) and organization networks consistently show high levels of concentration of citations in a few of the discovered clusters. Our results demonstrate that the baseline modularity-based method may not be capable of fully capturing the way collaborations drive the spreading of inventive impact across technological domains. This is due to the presence of local hierarchies that call for more refined tools based on Bayesian inference.

PACS numbers: 89.75.Fb; 02.50.Tt

I. INTRODUCTION

Innovation is an outcome of the complex patterns characterizing the collaborations among inventors, firms and institutions [1–3] - which affect the way knowledge is created, recombined and diffused. While the detection of communities within scientific collaboration networks has a well-established tradition in the literature [4–6], much less attention has been devoted to studying the mesoscopic structure of *innovation networks*, the architecture of which not only reveals who collaborates with whom but also how knowledge circulates through the innovation system's modular organization [7].

Here, we examine the mesoscale of innovation networks in the three strategic sectors of *artificial intelligence* (AI), *biotechnology* (BT) and *semiconductors* (SC) - domains that are recognized as transformative and enabling the technologies that underpin Europe's, as well as the world's, innovation capacity and technological sovereignty [8, 9]. Although each of the aforementioned sectors contributes to the emergence of new technological paradigms, different coordination logics are obeyed:

AI advances through software-driven experimentations and data infrastructures [10, 11], BT evolves through academic-industrial alliances and life-science discoveries [12, 13] and SC rely on capital-intensive, hierarchical production systems [14–16]. In order to compare these heterogeneous 'innovation ecosystems', we consider the ORBIS IP patent data across the years 2020–2024 and construct the individual-level (co-inventorship) and organization-level (co-ownership) networks induced by the interconnections among the top-500 most influential actors in each sector, ranked by forward citations. This is a standard measure of technological impact [17]. The chosen threshold captures the densest and most influential segment of collaborations, while maintaining interpretability and cross-sector comparability¹.

Network theory provides a rigorous framework to represent and analyze such systems, where nodes and edges denote agents and their collaborations, respectively [18]. A defining feature of social networks - of which innovation networks are instances - is their tendency to exhibit assortative mixing and a high clustering [19], clues that *i*) individuals with a similar degree tend to connect

* tiziano.squartini@imtlucca.it

¹We also show that the obtained results are robust to alternative cut-offs (top-300 and top-700).

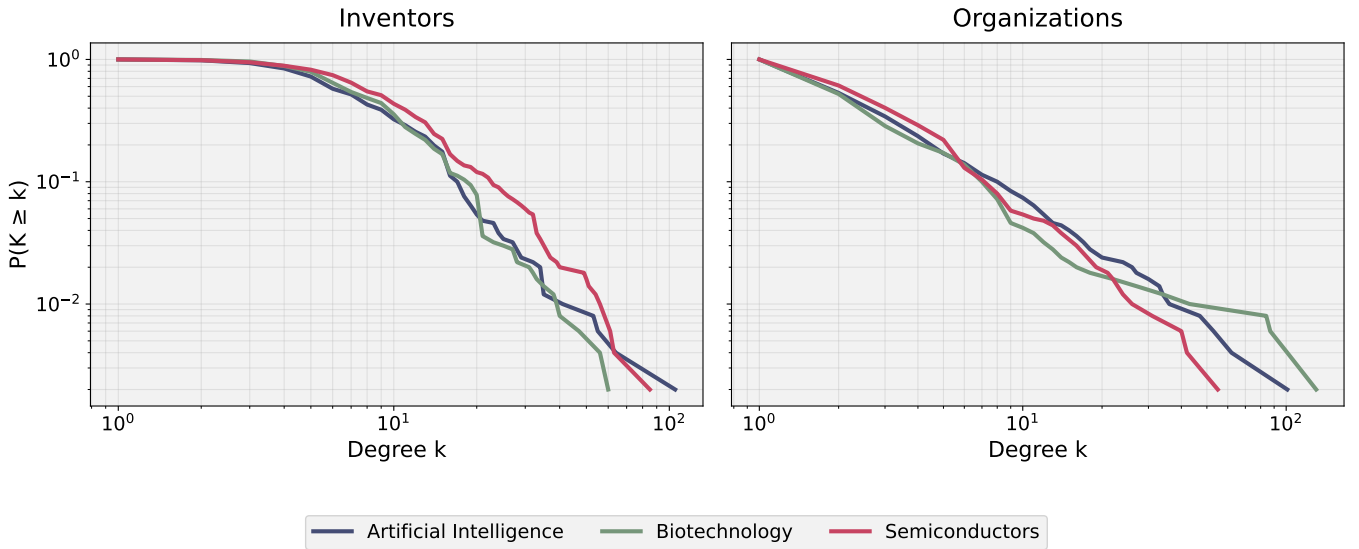


FIG. 1: **Local connectivity of innovation networks.** Complementary cumulative degree distributions of inventor (left) and organization (right) networks in the three, strategic sectors of artificial intelligence, biotechnology and semiconductors (only the top-500 actors have been considered). Across all sectors, organization-level networks exhibit heavier tails, a feature revealing the higher heterogeneity of the involved actors.

with each other; *ii*) individuals who collaborate with the same partners tend to form tightly knit groups. These structural signatures reflect the social and institutional embeddedness of knowledge creation [20, 21].

Between local interactions and global network properties lies a mesoscale level of organization, characterized by groups of nodes arranged in hierarchies of varying strength that collectively govern information flows, specialization and inequality [19, 22, 23]. Detecting these structures requires to go beyond the too simplistic notions of ‘dense’ and ‘central’ subgraph: state-of-the-art approaches treat such patterns as emergent properties and model them via probabilistic frameworks like the one of Exponential Random Graphs (ERGs) [24–27]. The adoption of statistically-grounded inference methods has allowed mesoscale structures detection to be rephrased in the jargon of model selection (and carried out by optimizing information criteria like the Minimum Description Length [26–29]), thus allowing genuine regularities - be they clusters, core-periphery structures, nested arrangements - to be distinguished from statistical noise.

We apply and systematically compare two alternative approaches to mesoscale structure detection - modularity maximization, a widely used baseline for community detection, and Bayesian Information Criterion (BIC) minimization, within the Stochastic Block Model (SBM) framework and its degree-corrected variant (dcSBM) - across six collaboration networks spanning three technological domains (artificial intelligence, biotechnology and semiconductors) and two organizational levels (inventors and organizations). We obtain three, major results: *i*) across all domains, inventor (co-inventorship) networks are consistently denser, more assortative and more clus-

tered than organization (co-ownership) networks, indicating the presence of relatively tight and recurrent collaboration circles. In contrast, organization networks exhibit a sparser, locally tree-like topology, consistent with hierarchical and role-differentiated structures; *ii*) when inspecting the mesoscale organization through the lens of the inference-based SBM framework (via BIC minimization), additional hierarchical and role-based patterns emerge that are not fully captured by modularity alone. When comparing these results with those from the baseline method, we find that modularity-based community detection alone is not sufficient to capture these hierarchical and role-based mesoscale patterns, which are instead recovered by the inference-based SBM framework: therefore, focusing exclusively on community structure can obscure organizational features that are central to understanding collaboration patterns in innovation networks; *iii*) differences in mesoscale organization are reflected in the distribution of inventive impact. Inequality in patent influence, measured using Lorenz curves of forward citations, is particularly pronounced in inventor networks across all sectors, indicating that a small fraction of inventors accounts for a disproportionate share of technological influence. Inequality is also evident at the organization level - most notably in the AI sector, where forward citations are concentrated in a limited number of dominant corporate-academic alliances - while BT and SC display comparatively more balanced patterns.

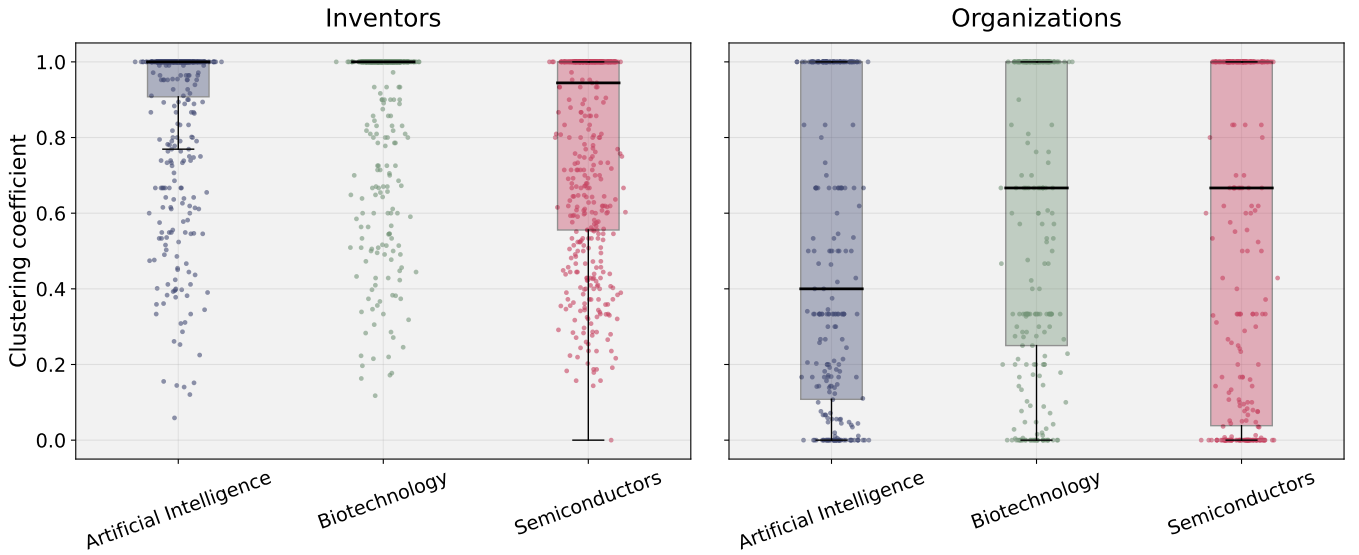


FIG. 2: Local cohesion of innovation networks. Distribution of the average clustering coefficient for inventor- and organization-level networks in the three, strategic sectors of artificial intelligence, biotechnology and semiconductors (only the top-500 actors have been considered). Inventor networks are more clustered than organization networks, a feature reflecting the prevalence of small, cohesive teams; organization networks, on the other hand, are more hierarchical, with few firms establishing many, diverse partnerships while most remain specialized.

II. RESULTS

The three results discussed in the introduction are treated in detail in each of the following subsections, respectively. In particular, in Section II A we describe innovation networks using aggregate, network-level metrics and highlight systematic differences between inventor- and organization-level collaborations. In Section II B we investigate the mesoscale organization of these networks by applying two alternative approaches, namely modularity maximization and BIC minimization, within the SBM framework and its degree-corrected variant. Finally, in Section II C we relate the detected structures to innovation outcomes, assessing how technological impact (measured through citations) is distributed across clusters.

A. Innovation networks at the macroscale

Across the three domains, inventor networks are consistently denser than organization networks: while the density of the former reads $\rho_{\text{AI}}^i \simeq 0.018$, $\rho_{\text{BT}}^i \simeq 0.018$ and $\rho_{\text{SC}}^i \simeq 0.022$, the density of the latter reads $\rho_{\text{AI}}^o \simeq 0.007$, $\rho_{\text{BT}}^o \simeq 0.007$ and $\rho_{\text{SC}}^o \simeq 0.007$; besides, the degree distributions of all networks are heavy-tailed (see fig. 1), a feature indicating the coexistence of highly connected nodes with many, poorly connected ones - and consistent with the bursty, heterogeneous dynamics typical of human systems [30]: yet, organization networks are characterized by steeper tails whereas inventor networks dis-

play a more homogeneous structure. Finally, the average clustering coefficient of inventor networks is higher than that of organization networks (see fig. 2).

These observations are confirmed by the metrics reported in table I: inventor networks display a moderate dispersion of degree values ($\text{CV} \lesssim 1$) and a high Nakamoto index [31, 32], indicating that collaborations are quite evenly distributed across individuals; organization networks, instead, exhibit a higher heterogeneity ($\text{CV} > 1$) and a markedly lower Nakamoto index (approximately half the one of inventor networks), signaling that an overall small subset of firms accounts for the majority of collaborative ties.

Taken together, the aforementioned results depict *i*) inventor networks as characterized by small teams originating distributed collaborations; *ii*) organization networks as less cohesive and more hierarchical, with few firms maintaining many partnerships that span institutional boundaries, while most remain specialized or, at least, regionally confined.

B. Innovation networks at the mesoscale

In order to assess how the structure of collaborations shapes the technological influence, we implement two algorithms for detecting mesoscale structures, i.e. the maximization of the modularity and the minimization of BIC, instantiated with the SBM and the dcSBM.

As fig. 3 shows, modularity maximization leads to identify clusters of densely-interconnected actors; the minimization of BIC instantiated with the SBM, on the other

Sector	Level	N	L	\bar{k}	σ_k	σ_k/\bar{k}	Nakamoto index
AI	Inv.	300	2931	19.54	19.50	1.00	71
		500	2252	9.01	8.39	0.93	119
		700	5367	15.33	17.47	1.14	133
BT	Inv.	300	1318	8.79	6.55	0.75	78
		500	2300	9.20	6.98	0.76	131
		700	3497	9.99	9.18	0.92	166
SC	Inv.	300	1640	10.93	9.83	0.90	67
		500	2803	11.21	9.80	0.87	119
		700	4801	13.72	12.78	0.93	145
AI	Org.	300	665	4.43	7.11	1.60	35
		500	923	3.69	7.38	1.99	52
		700	1434	4.10	8.35	2.04	76
BT	Org.	300	673	4.49	12.63	2.82	34
		500	888	3.55	9.59	2.70	49
		700	1496	4.27	12.29	2.88	71
SC	Org.	300	488	3.25	4.54	1.40	47
		500	870	3.48	4.96	1.43	82
		700	1229	3.51	4.81	1.37	114

TABLE I: **Network-level inequality metrics.** Indicators of structural inequality for inventor- and organization-level networks in the three, strategic sectors of artificial intelligence, biotechnology and semiconductors. Columns include the number of nodes (N), the number of edges (L), the average degree (\bar{k}) and the degree standard deviation (σ_k), the coefficient of variation ($CV = \sigma_k/\bar{k}$) and the Nakamoto index. While inventor networks are moderately unequal (low CV and high Nakamoto index), organization networks are much more so (high CV and low Nakamoto index) - in other words, while many individuals collaborate, few firms concentrate the majority of ties. At the sector-level, inequality is more pronounced in AI and BT.

hand, leads to a sharper distinction between hubs and peripheral actors, a picture that is further refined by instantiating BIC with the dcSBM. Employing inferential techniques leads to spot tree-like architectures, i.e. dense cores surrounded by semi-independent branches, that mirror a role-based partition of the system under consideration.

Such a picture is further refined by the results shown in fig. 4: by scattering the Shannon entropy of International Patent Classification (IPC) codes versus the number of distinct patent owners, one is able to assess the internal composition of the inventors' modules in terms of both organizational and technological diversity, i.e. whether they correspond to intra-firm/cross-firm collaborations (horizontal dimension) and whether their inventive activity is technologically specialized/generalist (vertical dimension). The share of single-company modules is small (below 25% in AI and BT and virtually absent in SC), a feature reflecting the cross-institutional character of innovation; in terms of technological scope, most modules fall above the median, thus corresponding to generalist groups spanning several technological subfields.

To be noticed that the clusters returned by modularity maximization tend to be concentrated in the upper-right quadrant, thus revealing inter-company and technologi-

cally diverse collaborations; the clusters returned by BIC minimization, instead, display a higher variability, with a subset of smaller, specialized ones alongside larger, multi-firm groups.

As fig. 5 shows, organization networks display a mesoscale architecture constituted of locally core-periphery structures. The metrics reported in table II further detail such a description. Under modularity maximization, the clusters display the strongest internal cohesion - the IC/EC ratio is, in fact, the largest. Minimizing BIC instantiated with the SBM yields less cohesive clusters and the lowest degree standard deviation, thus revealing the presence of peripheries centered around few, influential core-nodes; employing the degree-corrected variant of the SBM reconciles the two pictures above, as less clusters than modularity are recovered, showing, however, a more pronounced hierarchical structure (see also fig. 6, further clarifying the relationship between the structures detected by BIC-SBM and those detected by BIC-dcSBM).

Table III provides a comparative overview of the structures identified by our detection algorithms. In particular, *i*) organizations within the AI sector tend to form hub-driven, national systems dominated by Chinese and Korean conglomerates (Huawei, KAIST, Samsung); *ii*) organizations within the BT sector feature regionally-cohesive industrial complexes, such as the Sinopec-CNPC-CNOOC and the Sichuan-Zhejiang biomedical clusters; *iii*) organizations within the SC sector display hierarchical supply chains linking major equipment producers with integrated device manufacturers (IBM, Soitec-CEA-STMicro, TEL).

C. Inequality of the innovation impact

In order to quantify the distribution of the innovation impact across collaboration structures, let us plot the Lorenz curves of forward citations, a well-established measure of inequality that reveals the extent to which technological influence is concentrated. As fig. 7 shows, all inventor networks are characterized by the same trend, indicating that a small subset of communities is responsible for most of the technological influence - regardless of the sector. At the level of organizations, however, sectoral differences emerge: AI consistently exhibits the steepest Lorenz curves - i.e. the strongest concentration of forward citations - followed by BT and SC; this, in turn, suggests that (more than in other sectors) innovation is dominated by few alliances, acting as 'attractors' of citations. These patterns are fully consistent with the Gini coefficients reported in appendices and quantify the same underlying inequality with a single scalar.

Importantly, the 'magnitude' of inequality is affected by the algorithm employed to detected mesoscale structures: modularity maximization, for example, yields flatter curves for BT and sharper curves for SC. These patterns are due to the fact that modularity tends to split

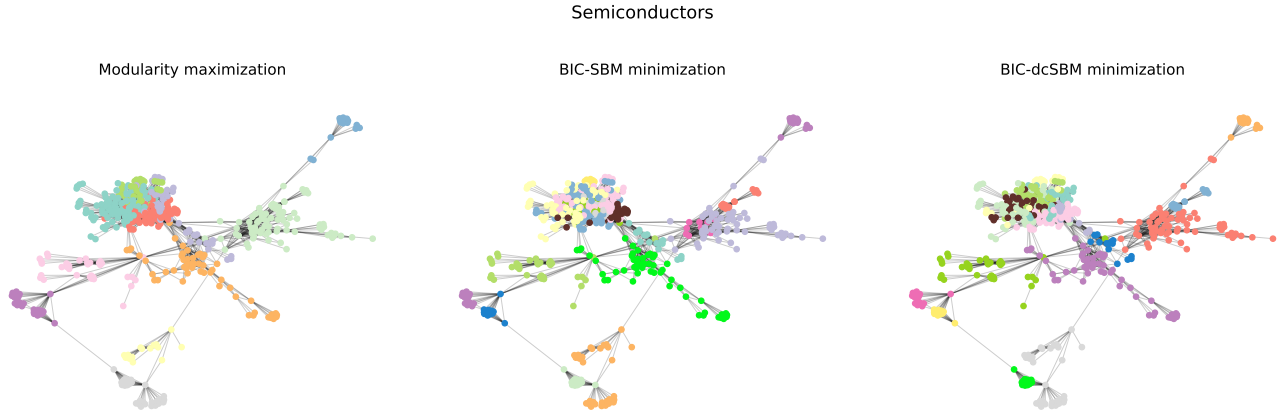


FIG. 3: **Mesoscale structure of the co-inventorship network in the semiconductor sector.** The higher density and average clustering coefficient characterizing inventor networks reflect into a pronounced modular structure that points out field-specific specializations leading to project-based collaborations: this, in turn, suggests that knowledge recombines through phases of concentrated teamwork within communities.

networks into smaller and more homogeneous clusters, thus dispersing high-impact patents across several groups of nodes. BIC minimization, on the contrary, leads to gather highly-connected, influential actors into cohesive cores, thereby capturing hierarchical, role-based patterns of knowledge accumulation that, in turn, causes the appearance of steeper curves.

III. DISCUSSION

As revealed by our results, collaborations shape innovation networks according to two, complementary dynamics that operate at different levels. This duality reflects the nested architecture typical of innovation ecosystems, where micro-level creative recombination unfolds within meso-level institutional structures that govern coordination and diffusion [33]. Such a multi-scale organization is a hallmark of complex socio-technical systems, in which inventive activity emerges from the interplay between cohesive teams and hierarchical organizational backbones.

At the individual level, knowledge production occurs through cohesive, recurrent teams: these structures suggest the importance of small, trusted groups for experimentation and rapid problem-solving - an attitude that is consistent with the project-based nature of inventive activity. These findings align with prior research showing that existing social ties, team cohesion and repeated collaborations enhance coordination and commercialization outcomes in inventive work [34–36]; besides, inventor teams that balance internal trust with disciplinary diversity tend to generate more valuable patents [37, 38]. Moreover, the high clustering observed in inventor networks is consistent with sociological evidence showing that small-world structures enhance collaborative cre-

ativity by balancing local cohesion and global reach [39]. This pattern assumes relevance in the light of some broader shifts in knowledge production, where teams, rather than individuals, have proven to become the dominant drivers of innovation [40].

At the organization level, instead, networks are sparser and more hierarchical: few, central agents (firms and institutions) connect otherwise weakly-linked actors, thus constituting the structural backbone upon which technological coordination rests. The aforementioned distinction is in line with previous studies indicating that co-assignment and R&D alliances often reflect strategic coordination across institutional boundaries rather than direct, interpersonal ties [41]. These hierarchical structures resonate with the well-documented dynamics through which star-firms and elite academic institutions exert disproportionate influence on emerging technological domains, shaping both the direction and the pace of innovation [42]. In this sense, organizational cores in AI and BT function as attractors of knowledge flows, mirroring the role of star-scientists and star-organizations in the formation of high-impact technological clusters. This dual structure (cohesive inventor teams embedded within sparser, hierarchical organizations) creates a nested architecture for innovation: at the team-level, dense, interpersonal ties support exploitation, thus enabling rapid iteration and refinement of ideas, i.e. efficient problem-solving; at the organization-level, central hubs connect otherwise separate groups, thus facilitating exploration through cross-cluster search, recombination of knowledge and access to diverse, technological inputs [39, 43, 44].

The analysis of Lorenz curves confirms that inequality in technological impact is pervasive, yet the extent to which it affects sectors varies: inventor networks are highly unequal, a result indicating that there are few, influential teams of highly-cited inventors. This finding is consistent with previous evidence that repeated collabora-

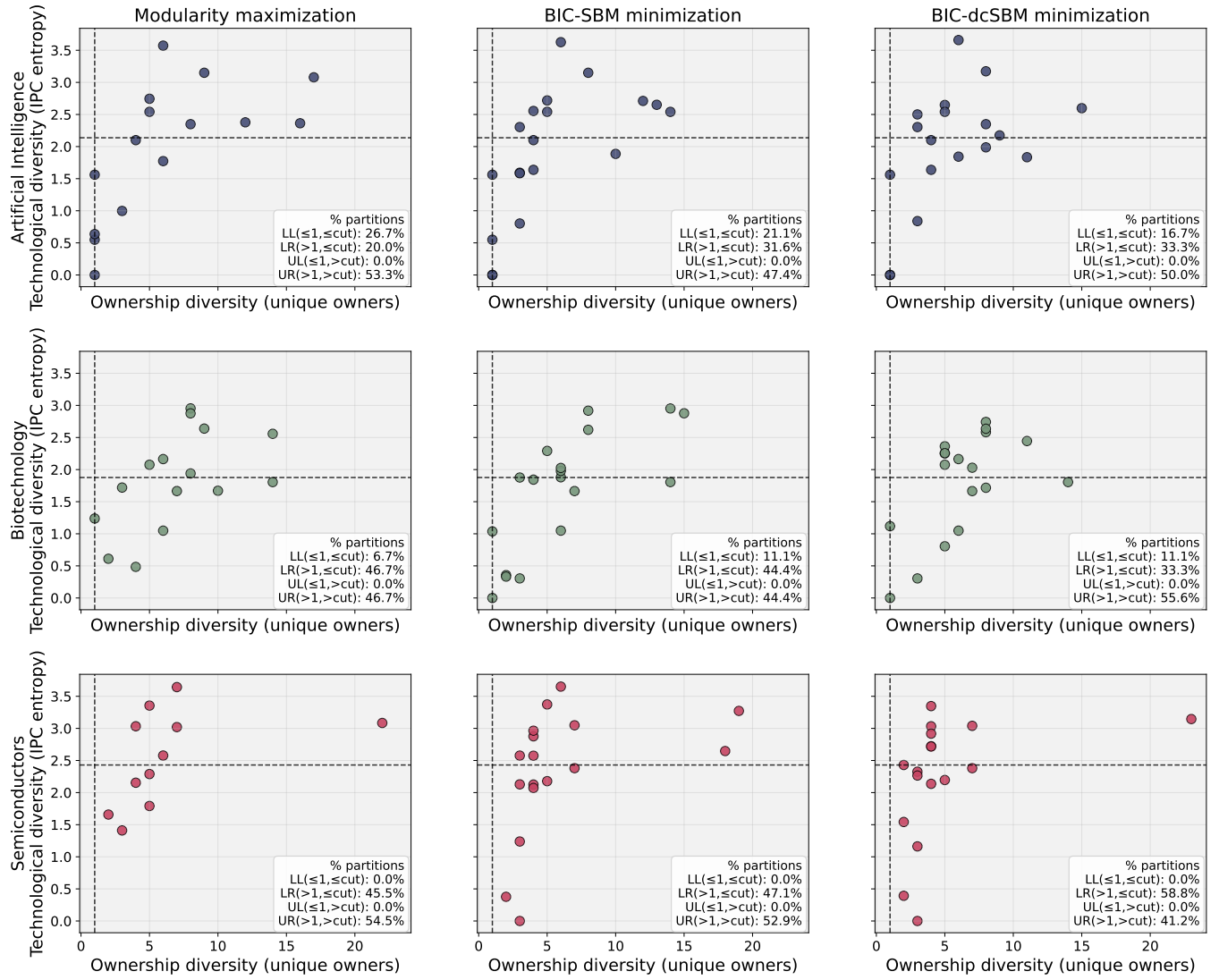


FIG. 4: Diversity of the inventors' modules across sectors and models. Each point represents a cluster of the top-500 inventor networks in the three, strategic sectors of artificial intelligence (top row), biotechnology (middle row) and semiconductors (bottom row), according to modularity maximization (left column), BIC minimization instantiated with the SBM (middle column) and BIC minimization instantiated with the dcSBM (right column). Ownership diversity (i.e. the number of distinct patent owners), distinguishing single-company from multi-company clusters, is reported on the x -axis; technological diversity (i.e. the Shannon entropy of IPC codes), distinguishing specialized from generalist clusters, is reported on the y -axis. Dashed lines mark the relevant thresholds: Shannon entropy is split at its median value; organizational diversity is split at $D_{\text{own}} = 1$; the bottom-right boxes report the percentage of partitions falling into each quadrant. Across all sectors, modules of inventors are predominantly inter-company and generalist, a feature indicating that inventive collaborations typically involve multiple organizations. To be noticed that modularity maximization leads to individuate broader, more diverse clusters than BIC minimization.

relations reinforce network persistence and cumulative advantage among established inventors [35]. At the level of organizations, inequality is most pronounced in the AI sector, where few corporate-academic alliances dominate, attracting a disproportionate share of forward citations; the BT and SC sectors, instead, display more balanced distributions. The steeper Lorenz curves observed for AI indicate a more pronounced concentration

of technological influence, consistent with cumulative-advantage mechanisms such as the Matthew effect [45]. While our networks are static and do not allow us to identify dynamic attachment processes directly, the resulting inequality patterns mirror those typically generated by preferential-attachment dynamics in innovation systems.

Finally, let us notice that different algorithms for mesoscale structures detection return different results:

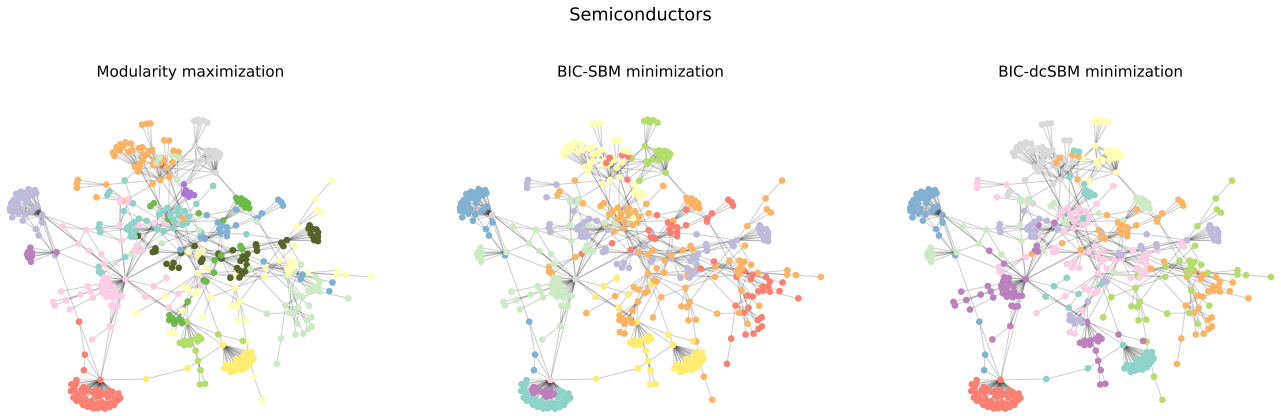


FIG. 5: **Mesoscale structure of the co-ownership network in the semiconductor sector.** Differently from inventor networks, organization networks are much less modular, appearing as combinations of core-periphery structures: while few firms maintain many cross-institutional partnerships, most actors remain specialized or, at least, regionally confined; this, in turn, suggests that knowledge flows across communities in a hierarchical fashion.

while modularity maximization tends to fragment the network into smaller clusters, thus distributing citations more evenly, BIC minimization is capable of individuating locally-hierarchical structures on the cores of which impact is concentrated.

IV. CONCLUSIONS

Taken together, our findings show that the architecture of innovation networks plays a central role in shaping how technological knowledge is created, coordinated and diffused across the global patent system. Across sectors, collaboration structures consistently reveal a dual pattern: at the inventor level, cohesive groups of individuals connect across organizational and technological boundaries, while at the organizational level, sparser and more hierarchical structures emerge, with a limited number of central actors coordinating wider ecosystems.

As of inventors, the clusters represent collaborations linking actors across organizational and technological boundaries. These groups do not necessarily represent enduring teams, mirroring, instead, the project-based character of inventive activity, where individuals from different firms cooperate on technologies of varying scope. Speaking of organizations, instead, the locally hierarchical patterns detected by our algorithms are especially pronounced in the AI sector, where national and corporate cores dominate the landscape of collaborations, while the BT and the SC sectors exhibit more regionally anchored and supply chains-oriented structures.

Several limitations of the present work should also be acknowledged. The present analysis focuses on the 500 most cited actors, thus providing an overview of the higher-impact segment while excluding emerging innovators. Our networks, summarizing collaborations across

the years 2020-2024, are also treated as static and, therefore, do not capture temporal changes in the composition of communities. Future work will extend this analysis longitudinally to study how mesoscale structures evolve (merge, fragment) and explore how events like policy interventions and technological shocks alter the balance between cohesion and hierarchy. Extending this analysis to a multi-layer representation that combines co-inventorship, co-ownership and citation networks would also allow us to gain a more complete view of the interdependencies sustaining the flowing of knowledge.

In conclusion, this study shows that innovation networks are hierarchical systems where collaborations and technological influence are deeply intertwined: cohesive inventor teams sustain the creation of knowledge at a microscopic level, while organizational hierarchies coordinate and amplify that knowledge; understanding the mesoscale architecture of collaboration networks is, therefore, crucial for understanding how they shape the distribution of inventive impact within and across technological domains.

V. MATERIALS AND METHODS

A. Network construction

Here, we focus on the most recent five-year period (from January 1, 2020 - December 31, 2024) to capture contemporary patterns of technological collaboration, while avoiding structural distortions due to older and less comparable data. We build three, sectorial collaboration networks - in the domains of *artificial intelligence*, *biotechnology* and *semiconductors* - where nodes represent either *patent inventors* or *patent owners* and binary, undirected edges connect entities that co-appear

Sector	Level	Algorithm	# clusters	\bar{k}_{within}	σ_k^{within}	IC/EC	BIC-SBM	BIC-dcSBM	Q
AI	Inventors	Modularity maximization	15	8.41	6.11	11.42	12878.44	15473.80	0.8404
		BIC-SBM minimization	20	18.09	5.48	3.88	11202.85	-	0.7145
		BIC-dcSBM minimization	17	9.77	6.34	5.10	-	14600.52	0.7890
	Organizations	Modularity maximization	9	3.32	6.36	11.56	8234.95	10803.32	0.7264
		BIC-SBM minimization	12	22.75	4.15	3.46	6404.86	-	0.2830
		BIC-dcSBM minimization	9	3.62	7.18	7.35	-	10787.43	0.6942
BT	Inventors	Modularity maximization	15	9.42	5.82	11.94	12406.82	15400.75	0.8498
		BIC-SBM minimization	19	1.49	2.78	0.72	5739.71	-	0.3200
		BIC-dcSBM minimization	18	9.85	5.93	7.22	-	14957.47	0.8232
	Organizations	Modularity maximization	9	3.96	8.06	2.64	8532.56	10116.84	0.6856
		BIC-SBM minimization	14	26.31	5.24	0.52	6141.66	-	0.2616
		BIC-dcSBM minimization	9	3.68	8.66	2.13	-	10105.29	0.6532
SC	Inventors	Modularity maximization	11	10.45	8.18	13.58	17665.27	30009.80	0.7073
		BIC-SBM minimization	17	14.06	6.89	2.49	15524.97	-	0.5160
		BIC-dcSBM minimization	19	11.32	8.61	3.95	-	18869.03	0.6662
	Organizations	Modularity maximization	15	3.47	4.43	7.34	7725.65	11250.47	0.8309
		BIC-SBM minimization	12	11.19	3.12	3.40	7128.25	-	0.6933
		BIC-dcSBM minimization	11	3.65	4.79	6.49	-	11132.57	0.8150

TABLE II: **Clusters diversity across sectors, levels and models.** As the ratio between the partition-specific numbers of intra-cluster and inter-cluster edges (IC/EC) reveals, inventor clusters are far more internally cohesive than organization clusters. More specifically, the maximization of modularity Q leads to recover clusters displaying the highest internal cohesion. Implementing the BIC-SBM, instead, leads to recover the least-cohesive clusters, in turn featuring the lowest within-cluster degree standard deviation $\sigma_k^{\text{within}} = R^{-1} \sum_{r=1}^R \sigma_k^r$ - a signature of the presence of peripheries centered around few cores. Finally, the BIC-dcSBM reconciles these two pictures, leading to recover fewer clusters than modularity, however displaying a more pronounced hierarchical structure.

on at least one patent.

Sectorial delineation follows the classification scheme detailed in Appendix A. Patent-level data are retrieved from the *ORBIS Intellectual Property* (ORBIS IP) database by Moody's [46], a comprehensive source linking global patent data to firm-level information, ownership structures and corporate networks². ORBIS IP integrates over 138 million patents with data on approximately 2.4 million companies worldwide, including ownership timelines, litigation cases, M&A information, patent valuations and technology classifications (IPC, CPC, USPC).

We focus on the most influential actors, restricting the analysis to the top-500 nodes ranked by forward citations. Our choice is also consistent with the strengths of ORBIS, particularly well-suited to analyze large and high-performing firms, global statistics and frontier-level innovation dynamics [48]. For robustness, we have replicated the analysis on the networks defined by the top-300 and the top-700 nodes for both inventors and organizations: results are stable upon varying the threshold.

B. Network analysis at the macroscale

We characterize each collaboration network, the adjacency matrix of which will be indicated as $\mathbf{A} = \{a_{ij}\}_{i,j=1}^N$, through the following properties [18]: upon indicating the total number of nodes with N and the total number of edges with L , one can define the link density as

$$\rho = \frac{2L}{N(N-1)}; \quad (1)$$

a high value of link density indicates more pervasive interconnections and is often associated with mature, or well-integrated, technological fields.

The number of neighbors of node i is captured by the degree $k_i = \sum_{j=1}^N a_{ij}$. From it, we can compute the average degree $\bar{k} = N^{-1} \sum_{i=1}^N k_i$ and the degree standard deviation $\sigma_k = \sqrt{N^{-1} \sum_{i=1}^N (k_i - \bar{k})^2}$, the ratio of which quantifies the relative dispersion of collaborations: values of the coefficient of variation $CV = \sigma_k/\bar{k}$ exceeding 1 indicate that the first moment is not representative of the distribution or, equivalently, that such a distribution can be considered as representing a heterogeneous system. The concentration of connectivity can be further assessed by computing the Nakamoto index, i.e. the minimum number of nodes, ranked by degree, required to account for the 51% of the total number of connections [31, 32]: smaller values indicate more unequal distributions dominated by few hubs.

²Although ORBIS and ORBIS IP are commercial datasets, requiring subscription-based access, their richness and data quality make them among the most widely-used sources for research in intellectual property, finance and economics [47].

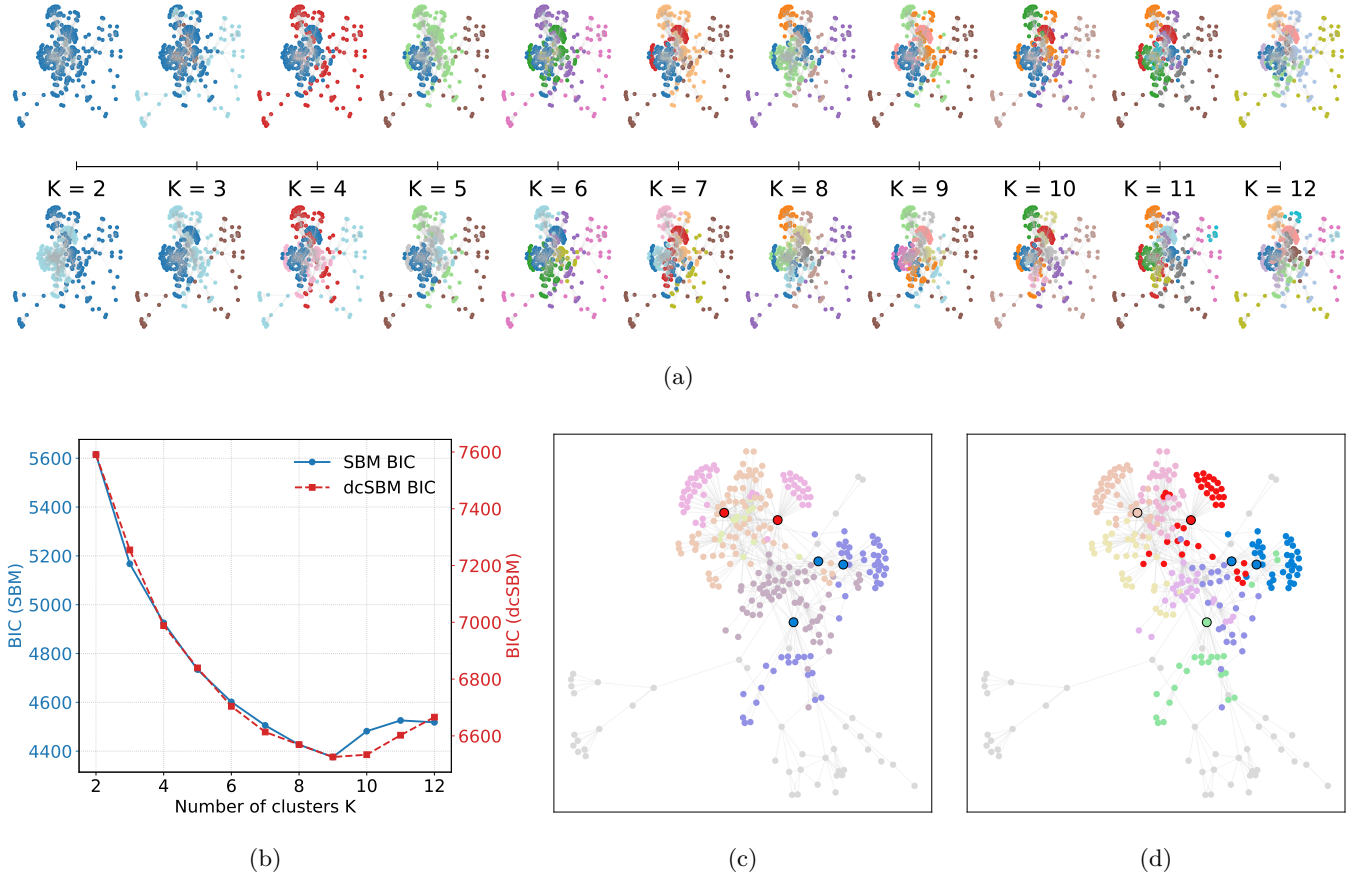


FIG. 6: **BIC-based partition of the co-inventorship network in the sector of artificial intelligence.** Panel (a) depicts the BIC-SBM partition (top row) and the BIC-dcSBM partition (bottom row) on the same layout, thus making it possible to appreciate how the two models refine the same tree-like structure as the number of clusters, K , increases. Panel (b) reports the BIC values as a function of K : for both models, the minimum lies at $K = 9$. Panels (c) and (d) illustrate this common optimum: in both cases, only part of the core-nodes (enlarged and contoured), as well as the periphery-nodes directly attached to them, are colored: under the BIC-SBM, they constitute small communities, the peripheries being assigned to separate blocks; under the BIC-dcSBM, instead, these nodes are put together. To reduce the computational burden, the analysis shown here has been carried out on the top-300 co-inventorship network.

The extent to which a collaboration network is cohesive can, instead, be quantified by computing the average clustering coefficient $\bar{c} = N^{-1} \sum_{i=1}^N c_i$, where

$$c_i = \frac{2t_i}{k_i(k_i - 1)}, \quad (2)$$

with $t_i = \sum_{j=1}^N \sum_{k(>j)} a_{ij} a_{jk} a_{ki}$ indicating the number of triangles incident to node i .

Finally, the degree distribution and the clustering coefficient distribution read $P(k) = N^{-1} \sum_{i=1}^N \mathbf{1}\{k_i = k\}$ and $P(c) = N^{-1} \sum_{i=1}^N \mathbf{1}\{c_i = c\}$. The degree distribution reveals the heterogeneity of collaborations, with heavy tails indicating the presence of few hubs alongside many, peripheral vertices; the clustering coefficient distribution quantifies the heterogeneity of local cohesion, thus complementing the aforementioned information.

C. Network analysis at the mesoscale

The problem of community detection has been extensively studied, leading to the development of numerous methods: among these, optimization-based approaches are, by far, the most popular ones.

1. Maximization of the modularity

The first, and most representative, method of the aforementioned class is the one prescribing to maximize modularity, defined as

$$Q = \frac{1}{2L} \sum_{i=1}^N \sum_j \left(a_{ij} - \frac{k_i k_j}{2L} \right) \delta_{g_i g_j}, \quad (3)$$

Sector	Modularity maximization	BIC-SBM minimization	BIC-dcSBM minimization
AI	9 clusters. Hub-driven, national innovation systems (China, Korea), dominated by large corporate-academic clusters such as Huawei, Samsung and KAIST	12 clusters. Role-based segmentation distinguishing the Guangdong digital, Korean industrial and State Grid-infrastructure ecosystems, plus a transnational academic-corporate hub	9 clusters. Degree correction merges subcommunities into cohesive, national macro-blocks (Guangdong, Korea, State Grid), revealing mirroring core-periphery structures
BT	9 clusters. Dense, regional and corporate clusters (Sinopec-CNPC-CNOOC, Sichuan, Zhejiang), shaped by geographic and industrial proximity	14 clusters. Finer, functional segmentation within corporate groups, distinguishing production, R&D and regulatory divisions within the same industrial conglomerates	9 clusters. Coarse-grained macro-blocks such as the Sinopec industrial complex, the Sichuan translational biomedical hub and the Zhejiang R&D cluster
SC	15 clusters. Hub-dominated clusters mirroring large ecosystems (IBM, Soitec-CEA-STMicro, TEL, Toyota) and mixed tool-materials groupings	12 clusters. Role-based blocks separating functionally different clusters (IBM, imec-Leuven, Toshiba/Kioxia, Toyota/Denso and TEL)	11 clusters. Degree-correction identifies macro-structures by unifying IBM with the GlobalFoundries federation, the two-tier TEL system and the R&D cores of imec-Leuven and Soitec-CEA-STMicro

TABLE III: Comparative overview of the mesoscale structures detected by our algorithms on the organization networks. Each entry of the table reports the number of detected clusters and a concise description of them.

where $\delta_{g_i g_j}$ is the Kronecker-delta function, equaling 1 if nodes i and j belong to the same group (i.e. $g_i = g_j$) and 0 otherwise (i.e. $g_i \neq g_j$), and $p_{ij} = k_i k_j / 2L$ is the probability that i and j are connected under the Chung-Lu model [5, 49]. Therefore, maximizing Q identifies the partition characterized by the number of edges within groups exceeding, to the largest extent, what would be expected by chance.

Despite its widespread use, modularity maximization is affected by both conceptual and practical flaws. As shown in [50], and later confirmed in [51], a key limitation arises from the presence of a very rugged landscape: in other words, Q often admits many, distinct partitions corresponding to nearly-identical, high scores, hence lacking a clearly-identifiable global maximum. Furthermore, in [50] the authors demonstrate that even random graphs (i.e. without a modular structure) can display relatively high modularity scores, depending on their size and average degree.

A second, major issue is represented by the so-called *resolution limit* [52], whereby small, yet well-defined, communities may remain undetected, as the optimization procedure tends to merge them into larger groups. Such a problem is not specific to any network structure, as the size of the modules that Q fails to identify depends on L as well as on the number of intermodular connections.

Aware of the limitations of the modularity optimization, we have compared its performance with the one of inferential approaches [29, 53, 54].

2. Minimization of the Bayesian Information Criterion

BIC is an information criterion widely employed to compare statistical models [55]: it embodies a trade-off between accuracy and complexity, penalizing models with too many parameters. More formally, the BIC of a probabilistic model with log-likelihood \mathcal{L} is defined as

$$\text{BIC} = \kappa \ln n - 2\mathcal{L}, \quad (4)$$

where κ denotes the number of parameters to be tuned and n denotes the size of the system under consideration. Assuming that a given, real-world configuration is the output of a generative model probabilistic in nature, BIC minimization can be employed for mesoscale structures detection: in such a case, it would compare different partitions - not just those consisting of modules - and select the optimal one. In what follows, we will instantiate BIC with the Stochastic Block Model and its degree-corrected variant (see Appendix B for the calculations and Appendix C for the codes).

Stochastic Block Model (SBM). Formally, it reads

$$\mathcal{L}_{\text{SBM}} = \prod_{r=1}^k p_{rr}^{L_{rr}} (1 - p_{rr})^{\binom{N_r}{2} - L_{rr}} \cdot \prod_{r=1}^k \prod_{s(>r)} p_{rs}^{L_{rs}} (1 - p_{rs})^{N_r N_s - L_{rs}}, \quad (5)$$

where N_r is the number of nodes constituting block r , L_{rr} is the number of links within block r , L_{rs} is the number of links between blocks r and s , $\forall r < s$; the probability coefficients read $p_{rr} = 2L_{rr}/N_r(N_r - 1)$,

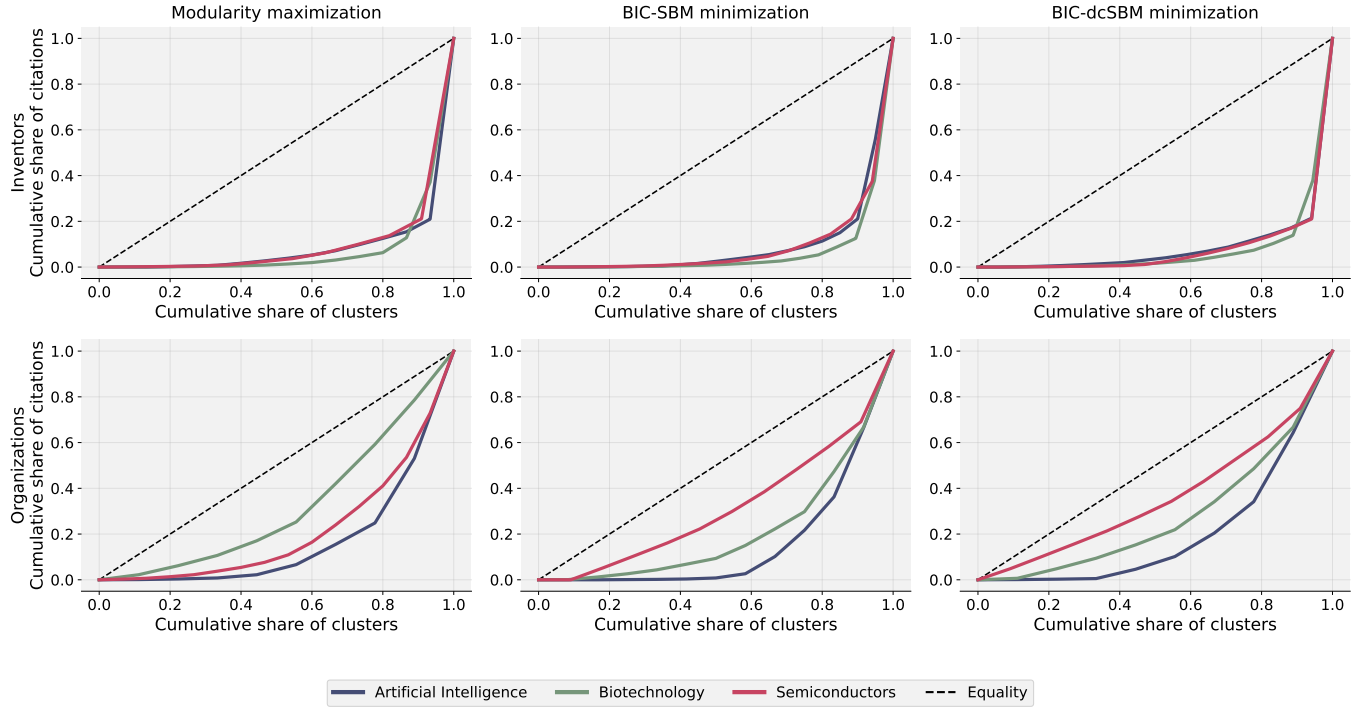


FIG. 7: **Inequality of the innovation impact.** Lorenz curves of forward citations for inventor and organization networks (only the top-500 actors have been considered). Inventor networks show a steadily high inequality across sectors, whereas organization networks are more diverse, with the AI sector exhibiting the highest level of inequality.

$r = 1 \dots k$ and $p_{rs} = L_{rs}/N_r N_s$, $\forall r < s$ (see Appendix B for the derivation of the SBM within the framework of the ERGs).

Degree-corrected Stochastic Block Model (dcSBM). Under the SBM, the nodes within the same block are treated as statistically equivalent. Real-world networks, however, are typically heterogeneous. In order to properly account for this, we have also considered the degree-corrected variant of the SBM, reading

$$\mathcal{L}_{\text{dcSBM}} = \sum_{i=1}^N \sum_{j(>i)} [a_{ij} \ln p_{ij} + (1 - a_{ij}) \ln(1 - p_{ij})], \quad (6)$$

where the generic probability coefficient is defined as

$$p_{ij} = \frac{x_i x_j \chi_{g_i g_j}}{1 + x_i x_j \chi_{g_i g_j}} \quad (7)$$

where x_i is the multiplier controlling for the degree of node i , x_j is the multiplier controlling for the degree of node j and $\chi_{g_i g_j}$ is the multiplier controlling for the link density between groups g_i and g_j (see Appendix B for the derivation of the dcSBM within the framework of the ERGs).

3. Characterization of the partitions

In order to describe the composition of the partition identified by each algorithm, we perform complementary analyses at the levels of individuals and organizations, further characterizing each cluster through a set of indicators that summarize its internal organization.

More specifically, we compute the cluster-specific average degree and degree standard deviation as well as the ratio between intra-cluster and inter-cluster connectivity, in symbols, IC/EC. While the first two quantities measure the average intensity of collaborations and the extent to which they are (un)evenly distributed across a cluster members, the IC/EC ratio is defined as the number of intra-cluster edges divided by the number of inter-cluster edges, thus capturing how sharply clusters are separated from the rest of the network: in words, high (low) values indicate communities less (more) integrated with the rest of the network.

Inventor-level. At the level of inventors, we assess the diversity of each cluster along two, complementary dimensions: *i*) the degree of *organizational diversity*, measured by the number of distinct patent owners within each cluster, $D_{\text{own}}^{(r)}$, and distinguishing *single-company* clusters ($D_{\text{own}}^{(r)} = 1$) from *multi-company* ones ($D_{\text{own}}^{(r)} > 1$); *ii*) the degree of *technological diversity*, measured through the Shannon entropy of IPC codes [56]. For each cluster r ,

let $p_c^{(r)}$ denote the share of patents classified under IPC code c ; the entropy is, then, defined as

$$D_{\text{IPC}}^{(r)} = - \sum_c p_c^{(r)} \ln p_c^{(r)}. \quad (8)$$

Shannon entropy is particularly suitable in this context since it does not simply count the number of distinct IPC classes - which would only reflect variety - but also captures how evenly patents are distributed across those classes [57]. It, therefore, increases when a cluster covers multiple technological domains with comparable intensity and decreases when patents are concentrated within a few IPC categories; besides, it represents a scale-independent measure of diversity that can be employed to carry out consistent comparisons across sectors and models. The combined use of the indicators above reveals whether a given cluster can be deemed as (primarily) representing intra-firm specialization, inter-firm collaborations, or multi-firm technological integration.

Organization-level. At the level of organizations, we perform a qualitative examination of the clusters detected by each algorithm: for every sector and model, the largest clusters have been manually inspected to identify their institutional composition, the dominant firms and the scope (either national or regional). This information is retrieved from patent assignee names and cross-checked with publicly available corporate and institutional affiliations. The resulting summary is reported in table III, providing a concise description of the structure captured by each algorithm (e.g. corporate clusters, national innovation systems, vertically-integrated industrial ecosystems).

D. Lorenz curves of forward citations

In order to quantify the heterogeneity of inventive impact across the mesoscale structure of each network, we compute the Lorenz curve [58] and Gini coefficient [59] for the corresponding distribution of patent forward citations. Given the model M and the network level ℓ (either inventors or organizations), let $f_c^{(r)}$ denote the total number of forward citations received by all patents associated with cluster $r = 1 \dots k_M^\ell$. Upon ordering clusters by increasing value of $f_c^{(r)}$, the cumulative shares read

$$X_j = \frac{j}{k_M^\ell}, \quad (9)$$

$$Y_j = \frac{\sum_{r=1}^j f_c^{(r)}}{\sum_{r=1}^{k_M^\ell} f_c^{(r)}} \quad (10)$$

and plotting the pairs (X_j, Y_j) yields the Lorenz curve, where X_j is the cumulative fraction of partitions and

Y_j the cumulative fraction of total citations. With an abuse of notation, the corresponding Gini coefficient is computed as

$$G = 1 - 2 \int_0^1 Y(X) dX; \quad (11)$$

while a perfectly equal distribution corresponds to $G = 0$, the value $G = 1$ indicates that all citations are concentrated in a single cluster (see Also Appendix D for the calculation of the curves on the top-300 and top-700 representations of our system).

VI. ACKNOWLEDGMENTS

This work has been supported by the projects: ‘RE-Net - Reconstructing economic networks: from physics to machine learning and back’ - 2022MTBB22, Funded by the European Union Next Generation EU, PNRR Mission 4 Component 2 Investment 1.1, CUP: D53D23002330006; ‘C2T - From Crises to Theory: towards a science of resilience and recovery for economic and financial systems’ - P2022E93B8, Funded by the European Union Next Generation EU, PNRR Mission 4 Component 2 Investment 1.1, CUP: D53D23019330001; ‘SoBigData RI PPP - SoBigData RI Preparatory Phase Project’, funded by the European Union under the scheme HORIZON-INFRA-2021-DEV-02-01, preparatory phase of new ESFRI research infrastructure projects, G.A. 101079043; ‘FAIR - Future Artificial Intelligence Research’ - Spoke 1 ‘Human-centered AI’, funded by the European Commission under the Next Generation EU program, PNRR Mission 4 Component 2 Investment 3.1, G.A. PE00000013; SMaRT CONSTRUCT (CUP J53C24001460006), in the context of FAIR (PE0000013, CUP B53C22003630006) under the National Recovery and Resilience Plan (Mission 4, Component 2, Line of Investment 1.3) funded by the European Union - NextGenerationEU.

The authors are grateful to the participants of the FAIR 2025 General Conference for their valuable feedback.

VII. CODE AND DATA AVAILABILITY

The Python package named **DOMINO** (*Detection Of Mesoscale structures via INFOrmation criteria*), implementing the algorithms described in the main text, is available on PyPI and at the URL <https://github.com/mattiamarzi/DOMINO>. The underlying patent-level data were obtained from Orbis Intellectual Property (Moody’s), a proprietary database subject to licensing restrictions, and therefore cannot be publicly shared.

VIII. AUTHOR CONTRIBUTIONS

Study conception and design: AM, AV, TS. Literature review: AG, LE. Data collection: AM, AV, LE. Analysis and interpretation of results: AG, AM, AV, LE, MM, TS. Draft manuscript preparation: AG, LE, MM, TS. Draft

manuscript revision: AG, AM, AV, LE, MM, TS. Python package preparation: MM.

IX. COMPETING INTERESTS

The authors declare no competing interests.

[1] W. W. Powell, K. W. Koput, and L. Smith-Doerr, *Administrative Science Quarterly* **41**, 116 (1996).

[2] C. Freeman, *Cambridge Journal of Economics* **19**, 5 (1995).

[3] B. Uzzi, *Administrative Science Quarterly* **42**, 35 (1997).

[4] M. Girvan and M. E. Newman, *Proceedings of the national academy of sciences* **99**, 7821 (2002).

[5] M. E. Newman, *Proceedings of the national academy of sciences* **103**, 8577 (2006).

[6] V. D. Blondel, J.-L. Guillaume, R. Lambiotte, and E. Lefebvre, *Journal of Statistical Mechanics: Theory and Experiment* **2008**, P10008 (2008).

[7] D. Acemoglu, U. Akcigit, and W. R. Kerr, *Proceedings of the National Academy of Sciences* **113**, 11483 (2016).

[8] T. Ramahandry, V. Bonneau, E. Bani, N. Vlasov, M. Flickenschild, O. Batura, N. Tcholtchev, P. Lämmel, and M. Boerger, *Key Enabling Technologies for Europe's Technological Sovereignty*, Tech. Rep. PE 697.184 (Panel for the Future of Science and Technology (STOA), European Parliamentary Research Service, Brussels, 2021).

[9] S. University, “Stanford emerging technology review 2025,” <https://setr.stanford.edu> (2025), accessed July 2025.

[10] R. Chellappa, G. Madhavan, T. E. Schlesinger, and J. L. Anderson, *PNAS Nexus* **4**, pgaf030 (2025).

[11] M. F. Safitra, M. Lubis, T. F. Kusumasari, and D. P. Putri, *Procedia Computer Science* **234**, 381 (2024).

[12] W. W. Powell, D. R. White, K. W. Koput, and J. Owen-Smith, *American Journal of Sociology* **110**, 1132 (2005).

[13] A. L. Oliver, *Research Policy* **33**, 583 (2004).

[14] R. Kapoor and P. J. McGrath, *Research Policy* **43**, 555 (2014).

[15] R. Huggins, A. Johnston, M. Munday, and C. Xu, *Science and Public Policy* **50**, 531 (2023).

[16] L. D. Browning, J. M. Beyer, and J. C. Shetler, *Academy of Management Journal* **38**, 113 (1995).

[17] B. H. Hall, A. B. Jaffe, and M. Trajtenberg, “Market value and patent citations: A first look,” (2000).

[18] M. E. J. Newman, *Networks: An Introduction*, 2nd ed. (Oxford University Press, Oxford, UK, 2018).

[19] M. E. Newman and J. Park, *Physical review E* **68**, 036122 (2003).

[20] S. Wasserman and K. Faust, *Social Network Analysis: Methods and Applications* (Cambridge university press, 1994).

[21] D. J. Watts, *Small worlds: the dynamics of networks between order and randomness* (Princeton university press, 1999).

[22] S. Fortunato and D. Hric, *Physics reports* **659**, 1 (2016).

[23] B. S. Khan and M. A. Niazi, arXiv preprint [arXiv:1708.00977](https://arxiv.org/abs/1708.00977) (2017), 10.48550/arXiv.1708.00977.

[24] J. Park and M. E. J. Newman, *Physical Review E* **70**, 66117 (2004).

[25] G. Bianconi, *Europhysics Letters* **81**, 28005 (2007).

[26] A. Fronczak, ArXiv (2012), [doi.org/10.48550/arXiv.1210.7828](https://arxiv.org/abs/1210.7828).

[27] T. Squartini and D. Garlaschelli, *Maximum-Entropy Networks. Pattern Detection, Network Reconstruction and Graph Combinatorics* (Springer International Publishing, 2017) p. 116.

[28] B. Karrer and M. E. Newman, *Physical Review E—Statistical, Nonlinear, and Soft Matter Physics* **83**, 016107 (2011).

[29] T. P. Peixoto, *Advances in network clustering and block-modeling*, 289 (2019).

[30] A.-L. Barabási, *Nature* **435**, 207 (2005).

[31] B. S. Srinivasan and L. Lee, “Quantifying decentralization,” <https://news.earn.com/quantifying-decentralization-e39db233c28e> (2017), accessed: YYYY-MM-DD.

[32] J. H. Lin, E. Marchese, C. J. Tessone, and T. Squartini, *Chaos, Solitons & Fractals* **164**, 112620 (2022).

[33] D. J. Jackson, *What is an Innovation Ecosystem*, Tech. Rep. 1(2) (National Science Foundation, Arlington, VA, 2011).

[34] J. Bercovitz and M. Feldman, *Research Policy* **40**, 81 (2011).

[35] G. Tóth, S. Juhász, Z. Elekes, and B. Lengyel, *European Planning Studies* **29**, 2252 (2021).

[36] R. Guimerà, B. Uzzi, J. Spiro, and L. A. N. Amaral, *Science* **308**, 697 (2005).

[37] H. Inoue, K. Nagayoshi, and K. Yamaguchi, *PLoS ONE* **10**, e0121973 (2015).

[38] A. M. Petruzzelli, D. Rotolo, and V. Albino, *Technological Forecasting and Social Change* **91**, 208 (2015).

[39] B. Uzzi and J. Spiro, *American Journal of Sociology* **111**, 447 (2005).

[40] S. Wuchty, B. F. Jones, and B. Uzzi, *Science* **316**, 1036 (2007).

[41] M. Fritsch, M. Piontek, and M. Titze, *Industry and Innovation* **27**, 630 (2020).

[42] L. G. Zucker and M. R. Darby, *Proceedings of the National Academy of Sciences* **93**, 12709 (1996).

[43] J. G. March, *Organization Science* **2**, 71 (1991).

[44] M. A. Schilling and C. C. Phelps, *Management Science* **53**, 1113 (2007).

[45] R. K. Merton, *Science* **159**, 56 (1968).

[46] Moody's Analytics, “Orbis intellectual property,” <https://orbisip-r1.bvdinfo.com/version-20250624-1-0/OrbisIntellectualProperty/1/Patents/Search> (2025).

[47] P. N. Gal, *Measuring Total Factor Productivity at the Firm Level using OECD-ORBIS*, OECD Economics

Department Working Papers 1049 (OECD Publishing, Paris, 2013).

[48] M. Bajgar, G. Berlingieri, S. Calligaris, C. Criscuolo, and J. Timmis, *Coverage and representativeness of Orbis data*, OECD Science, Technology and Industry Working Papers 2020/06 (OECD Publishing, Paris, 2020).

[49] F. Chung and L. Lu, *Annals of combinatorics* **6**, 125 (2002).

[50] R. Guimera, M. Sales-Pardo, and L. A. N. Amaral, *Physical Review E—Statistical, Nonlinear, and Soft Matter Physics* **70**, 025101 (2004).

[51] B. H. Good, Y.-A. De Montjoye, and A. Clauset, *Physical Review E—Statistical, Nonlinear, and Soft Matter Physics* **81**, 046106 (2010).

[52] S. Fortunato and M. Barthelemy, *Proceedings of the national academy of sciences* **104**, 36 (2007).

[53] T. P. Peixoto, *Physical Review X* **4**, 011047 (2014).

[54] T. P. Peixoto, *Physical Review E* **95**, 012317 (2017).

[55] K. P. Burnham and D. R. Anderson, *Model Selection and Multimodel Inference: A Practical Information-Theoretic Approach*, 2nd ed. (Springer, New York, NY, 2002).

[56] C. E. Shannon, *Bell System Technical Journal* **27**, 379 (1948).

[57] Y. Zhang, Y. Qian, Y. Huang, Y. Guo, G. Zhang, and J. Lu, *Scientometrics* **111**, 1925 (2017).

[58] M. O. Lorenz, *Publications of the American Statistical Association* **9**, 209 (1905).

[59] F. A. Cowell, *Measuring Inequality* (Oxford University Press, Oxford, UK, 2011).

[60] World Intellectual Property Organization, *WIPO Technology Trends 2019: Artificial Intelligence* (World Intellectual Property Organization, Geneva, 2019).

[61] N. Grassano, L. Napolitano, R. M'barek, E. Rodriguez Cerezo, and J. Lasarte Lopez, *Exploring the Global Landscape of Biotech Innovation: Preliminary Insights from Patent Analysis*, JRC137266 (Publications Office of the European Union, Luxembourg, 2024).

[62] P. Adams, R. Fontana, and F. Malerba, *Research Policy* **42**, 1 (2013).

[63] T. Squartini and D. Garlaschelli, *New Journal of Physics* **13**, 083001 (2011).

[64] M. Di Vece, E. Agrimi, S. Tatullo, T. Gili, M. Ibáñez-Berganza, and T. Squartini, *arXiv preprint arXiv:2508.00542* (2025), <https://arxiv.org/abs/2508.00542>.

[65] W. M. Rand, *Journal of the American Statistical Association* **66**, 846 (1971).

[66] P. Jaccard, *Bulletin de la Société Vaudoise des Sciences Naturelles* **37**, 547 (1901).

[67] L. Danon, A. Díaz-Guilera, J. Duch, and A. Arenas, *Journal of Statistical Mechanics: Theory and Experiment* **2005**, P09008 (2005).

Appendix A: Classification of Artificial Intelligence, Biotechnology and Semiconductors patents

To identify the patents belonging to artificial intelligence, biotechnology and semiconductor technologies, we adopted the following classification, ensuring that our sectorial delineation is consistent with prior work and internationally-recognized standards: AI patents were identified following the taxonomy of the *WIPO Technology Trends 2019: Artificial Intelligence* report [60], mapping CPC codes across AI subdomains such as computer vision, natural language processing and control methods; BT patents were identified following the taxonomy of the *Exploring the Global Landscape of Biotech Innovation* report by the European Commission Joint Research Center [61]; SC patents were identified following the IPC class H01L (semiconductor devices) proposed in [62]. An overview of the codes used to identify patents is provided in table IV.

Relevant CPC/IPC codes and categories	
Artificial intelligence	Computer vision and image processing: G06T1/20, G06T2207/20081, G06T2207/20084, G06T3/4046, G06T9/002 Augmented/mixed reality: G02B27/01, G06T19/006, G06F3/011, G05B2219/32014 Biometrics and character recognition: G06K9/00006, G06K9/00221, G06K2009/00395, G06K9/00375, G06K9/00597, G06K9/00885, G06K9/00362, G06K9/00335, G06K9/00402, G06K9/00442, G06K2209/01, G06K9/00852 Segmentation, tracking, scene understanding: G06T7/10, G06T7/215, H04N5/147, G06K9/34, H04N1/40062, G06F3/012, G06K2017/0045, G06T7/246, G08B13/2402, G06K9/00624, G06T1/0014, G06K9/00798 Control methods: G05B13/0265, G05B13/027, G05B13/0275, G05B13/028, G05B13/0285, G05B13/029, G05B13/0295, G05D1/0088 Natural language processing and knowledge representation: G06F17/279, G06F17/2765, G06F17/2705, G06F17/28, G06F17/30669, G06F17/2755, G06F17/2881, G06F17/2282, G06F17/30401, G06F17/3043, G06F17/30654, G06F17/30663, G06F17/30666, G06F17/30731, G06F17/2785, G06N5/00 Speech processing: G10L13/00, G10L15/00, G10L17/00, G10L25/00, G10L99/00, G06F17/30784
Biotechnology	A01H1/00, A01H4/00, A01K67/00, A61K35/12, A61K38/00, A61K38/17, A61K39/00, A61K39/395, A61K48/00, C02F3/34, C07G11/00, C07G13/00, C07G15/00, C07K4/00, C07K14/00, C07K16/00, C07K16/28, C07K17/00, C07K19/00, C12M1/00, C12M1/34, C12N15/82, C12N15/113, C12P, C12Q, C12Q1/68, C40B10/00, C40B40/02, C40B40/06, C40B40/08, C40B50/06, G01N27/327, G01N33/50, G01N33/53, G01N33/54, G01N33/543, G01N33/55, G01N33/57, G01N33/574, G01N33/68, G01N33/74, G01N33/76, G01N33/78, G01N33/88, G01N33/92, G06F19/10
Semiconductors	H01L

TABLE IV: CPC/IPC codes used to identify patents in Artificial Intelligence, Biotechnology and Semiconductors.

Appendix B: More on the Bayesian Information Criterion

The BIC reads

$$\text{BIC} = \kappa \ln n - 2\mathcal{L}, \quad (\text{B1})$$

where the symbols have been defined in the main text. Hereby, we instantiate it with the log-likelihood functions of the SBM and of the dcSBM. Both can be derived within the framework of ERGs, following the approach introduced in [24] and further developed in [63]. Such an approach looks for the probability distribution $P(\mathbf{A})$ that maximizes Shannon entropy

$$S = - \sum_{\mathbf{A} \in \mathbb{A}} P(\mathbf{A}) \ln P(\mathbf{A}), \quad (\text{B2})$$

where the sum runs over \mathbb{A} , i.e. the ensemble of all, possible binary, undirected graphs, under a set of constraints representing the expected values of certain properties. The formal solution to this problem reads

$$P(\mathbf{A}) = \frac{e^{-H(\mathbf{A})}}{Z} \quad (\text{B3})$$

where $H(\mathbf{A})$ is the Hamiltonian, i.e. a linear combination of the constrained properties, each multiplied by the corresponding Lagrange multiplier, and $Z = \sum_{\mathbf{A} \in \mathbb{A}} e^{-H(\mathbf{A})}$ is the partition function.

Stochastic Block Model (SBM). In the framework of ERGs, the SBM is defined by the Hamiltonian

$$H(\mathbf{A}) = \sum_{i=1}^N \sum_{j(>i)} \alpha_{g_i g_j} a_{ij} = \sum_{r=1}^k \sum_{s(\geq r)} \alpha_{rs} \sum_{i=1}^N \sum_{j(>i)} \delta_{g_i r} \delta_{g_j s} a_{ij} = \sum_{r=1}^k \sum_{s(\geq r)} \alpha_{rs} L_{rs}(\mathbf{A}), \quad (\text{B4})$$

where g_i denotes the group membership of node i . It induces the partition function reading

$$Z = \sum_{\mathbf{A} \in \mathbb{A}} e^{-H(\mathbf{A})} = \sum_{\mathbf{A} \in \mathbb{A}} \prod_{i=1}^N \prod_{j(>i)} e^{-\alpha_{g_i g_j} a_{ij}} = \prod_{i=1}^N \prod_{j(>i)} \sum_{a_{ij}=0,1} e^{-\alpha_{g_i g_j} a_{ij}} = \prod_{i=1}^N \prod_{j(>i)} [1 + e^{-\alpha_{g_i g_j}}]; \quad (\text{B5})$$

as a consequence, we have

$$\begin{aligned} P_{\text{SBM}}(\mathbf{A}) &= \frac{\prod_{i=1}^N \prod_{j(>i)} e^{-\alpha_{g_i g_j} a_{ij}}}{\prod_{i=1}^N \prod_{j(>i)} [1 + e^{-\alpha_{g_i g_j}}]} \\ &= \prod_{i=1}^N \prod_{j(>i)} \frac{x_{g_i g_j}^{a_{ij}}}{1 + x_{g_i g_j}} \\ &= \prod_{i=1}^N \prod_{j(>i)} p_{g_i g_j}^{a_{ij}} (1 - p_{g_i g_j})^{1-a_{ij}}, \end{aligned} \quad (\text{B6})$$

having posed $e^{-\alpha_{g_i g_j}} = x_{g_i g_j}$ and $p_{ij} = x_{g_i g_j} / (1 + x_{g_i g_j})$. Let us notice that

$$\begin{aligned}
P_{\text{SBM}}(\mathbf{A}) &= \prod_{i=1}^N \prod_{j(>i)} p_{g_i g_j}^{a_{ij}} (1 - p_{g_i g_j})^{1-a_{ij}} \\
&= \prod_{i=1}^N \prod_{j(>i)} \prod_{r=1}^k \prod_{s(>r)} [p_{rs}^{a_{ij}} (1 - p_{rs})^{1-a_{ij}}]^{\delta_{g_i r} \delta_{g_j s}} \\
&= \prod_{r=1}^k \prod_{s(>r)} \prod_{i=1}^N \prod_{j(>i)} \left[p_{rs}^{a_{ij} \delta_{g_i r} \delta_{g_j s}} (1 - p_{rs})^{\delta_{g_i r} \delta_{g_j s} (1-a_{ij})} \right] \\
&= \prod_{r=1}^k \prod_{s(>r)} \left[p_{rs}^{\sum_{i=1}^N \sum_{j(>i)} \delta_{g_i r} \delta_{g_j s} a_{ij}} (1 - p_{rs})^{\sum_{i=1}^N \sum_{j(>i)} \delta_{g_i r} \delta_{g_j s} (1-a_{ij})} \right] \\
&= \prod_{r=1}^k p_{rr}^{L_{rr}} (1 - p_{rr})^{\binom{N_r}{2} - L_{rr}} \prod_{s(>r)} p_{rs}^{L_{rs}} (1 - p_{rs})^{N_r N_s - L_{rs}}, \tag{B7}
\end{aligned}$$

where N_r is the total number of nodes in the r -th block, $r = 1 \dots k$. The parameters that define the SBM can be estimated by maximizing the log-likelihood

$$\mathcal{L}_{\text{SBM}} = \ln P_{\text{SBM}}(\mathbf{A}) = \sum_{r=1}^k \left[L_{rr}(\mathbf{A}) \ln x_{rr} - \binom{N_r}{2} \ln(1 + x_{rr}) \right] + \sum_{r=1}^k \sum_{s(>r)} [L_{rs}(\mathbf{A}) \ln x_{rs} - N_r N_s \ln(1 + x_{rs})] \tag{B8}$$

with respect to x_{rr} and x_{rs} . Upon doing so, we obtain the system of equations

$$\frac{\partial \mathcal{L}_{\text{SBM}}}{\partial x_{rr}} = \frac{L_{rr}(\mathbf{A})}{x_{rr}} - \binom{N_r}{2} \left(\frac{1}{1 + x_{rr}} \right), \tag{B9}$$

$$\frac{\partial \mathcal{L}_{\text{SBM}}}{\partial x_{rs}} = \frac{L_{rs}(\mathbf{A})}{x_{rs}} - N_r N_s \left(\frac{1}{1 + x_{rs}} \right) \tag{B10}$$

and equating them to zero leads to the conditions

$$p_{rr} = \frac{2L_{rs}(\mathbf{A})}{N_r(N_r - 1)}, \quad r = 1 \dots k \tag{B11}$$

$$p_{rs} = \frac{L_{rs}(\mathbf{A})}{N_r N_s}, \quad \forall r < s; \tag{B12}$$

as a consequence, BIC, now, reads $\text{BIC}_{\text{SBM}} = \kappa_{\text{SBM}} \ln n - 2\mathcal{L}_{\text{SBM}}$, with $\kappa_{\text{SBM}} = k(k+1)/2$.

Degree-corrected Stochastic Block Model (dcSBM). The dcSBM is, instead, defined by the Hamiltonian

$$H(\mathbf{A}) = \sum_{i=1}^N \sum_{j(>i)} \alpha_{ij} a_{ij} = \sum_{i=1}^N \sum_{j(>i)} (\alpha_i + \alpha_j + \alpha_{g_i g_j}) a_{ij}, \tag{B13}$$

leading to the partition function

$$\begin{aligned}
Z = \sum_{\mathbf{A} \in \mathbb{A}} e^{-H(\mathbf{A})} &= \sum_{\mathbf{A} \in \mathbb{A}} \prod_{i=1}^N \prod_{j(>i)} e^{-(\alpha_i + \alpha_j + \alpha_{g_i g_j}) a_{ij}} = \prod_{i=1}^N \prod_{j(>i)} \sum_{a_{ij}=0,1} e^{-(\alpha_i + \alpha_j + \alpha_{g_i g_j}) a_{ij}} = \prod_{i=1}^N \prod_{j(>i)} \left[1 + e^{-(\alpha_i + \alpha_j + \alpha_{g_i g_j})} \right], \tag{B14}
\end{aligned}$$

further implying

$$P_{\text{dcSBM}}(\mathbf{A}) = \frac{\prod_{i=1}^N \prod_{j(>i)} e^{-(\alpha_i + \alpha_j + \alpha_{g_i g_j}) a_{ij}}}{\prod_{i=1}^N \prod_{j(>i)} [1 + e^{-(\alpha_i + \alpha_j + \alpha_{g_i g_j})}]^a} = \prod_{i=1}^N \prod_{j(>i)} \frac{(x_i x_j \chi_{g_i g_j})^{a_{ij}}}{1 + x_i x_j \chi_{g_i g_j}}, \quad (\text{B15})$$

having posed $x_i = e^{-\alpha_i}$ and $\chi_{g_i g_j} = e^{-\alpha_{g_i g_j}}$. The parameters that define the dcSBM can be estimated by maximizing the log-likelihood

$$\begin{aligned} \mathcal{L}_{\text{dcSBM}} &= \ln P_{\text{dcSBM}}(\mathbf{A}) = \sum_{i=1}^N \sum_{j(>i)} [a_{ij} \ln(x_i x_j \chi_{g_i g_j}) - \ln(1 + x_i x_j \chi_{g_i g_j})] \\ &= \sum_{i=1}^N \sum_{j(>i)} \sum_{r=1}^k \sum_{s(\geq r)} \delta_{g_i r} \delta_{g_j s} [a_{ij} \ln(x_i x_j \chi_{rs}) - \ln(1 + x_i x_j \chi_{rs})] \end{aligned} \quad (\text{B16})$$

with respect to x_i and χ_{rs} . Upon doing so, we obtain the system of equations

$$\frac{\partial \mathcal{L}_{\text{dcSBM}}}{\partial x_i} = \sum_{j(\neq i)} \sum_{r=1}^k \sum_{s(\geq r)} \delta_{g_i r} \delta_{g_j s} \left(\frac{a_{ij}}{x_i} - \frac{x_j \chi_{rs}}{1 + x_i x_j \chi_{rs}} \right), \quad (\text{B17})$$

$$\frac{\partial \mathcal{L}_{\text{dcSBM}}}{\partial \chi_{rs}} = \sum_{i=1}^N \sum_{j(>i)} \delta_{g_i r} \delta_{g_j s} \left(\frac{a_{ij}}{\chi_{rs}} - \frac{x_i x_j}{1 + x_i x_j \chi_{rs}} \right) \quad (\text{B18})$$

and equating them to zero leads us to recover the conditions

$$k_i(\mathbf{A}) = \sum_{j(\neq i)} \sum_{r=1}^k \sum_{s(\geq r)} \delta_{g_i r} \delta_{g_j s} \left(\frac{x_i x_j x_{rs}}{1 + x_i x_j x_{rs}} \right), \quad i = 1 \dots N \quad (\text{B19})$$

$$L_{rs}(\mathbf{A}) = \sum_{i=1}^N \sum_{j(>i)} \delta_{g_i r} \delta_{g_j s} \left(\frac{x_i x_j \chi_{rs}}{1 + x_i x_j \chi_{rs}} \right), \quad \forall r \leq s; \quad (\text{B20})$$

as a consequence, BIC, now, reads $\text{BIC}_{\text{dcSBM}} = \kappa_{\text{dcSBM}} \ln n - 2\mathcal{L}_{\text{dcSBM}}$, with $\kappa_{\text{dcSBM}} = k(k+1)/2 + N$.

Since the resolution of the dcSBM is computationally demanding, here we have considered a ‘decoupled’ approximation of it, defined by the following algorithm. First, we have solved the Undirected Binary Configuration Model (UBCM) [24, 63], defined by the system of equations

$$k_i(\mathbf{A}) = \sum_{j(\neq i)} \left(\frac{x_i^{\text{UBCM}} x_j^{\text{UBCM}}}{1 + x_i^{\text{UBCM}} x_j^{\text{UBCM}}} \right), \quad i = 1 \dots N \quad (\text{B21})$$

afterwards, we have solved the system of equations

$$L_{rs}(\mathbf{A}) = \sum_{i=1}^N \sum_{j(>i)} \delta_{g_i r} \delta_{g_j s} \left(\frac{x_i^{\text{UBCM}} x_j^{\text{UBCM}} \chi_{rs}}{1 + x_i^{\text{UBCM}} x_j^{\text{UBCM}} \chi_{rs}} \right), \quad \forall r \leq s \quad (\text{B22})$$

with clear meaning of the symbols.

For additional evidence of the mesoscale structure of co-inventorship and co-ownership networks across sectors and levels, see fig. 8, fig. 9 and table V.

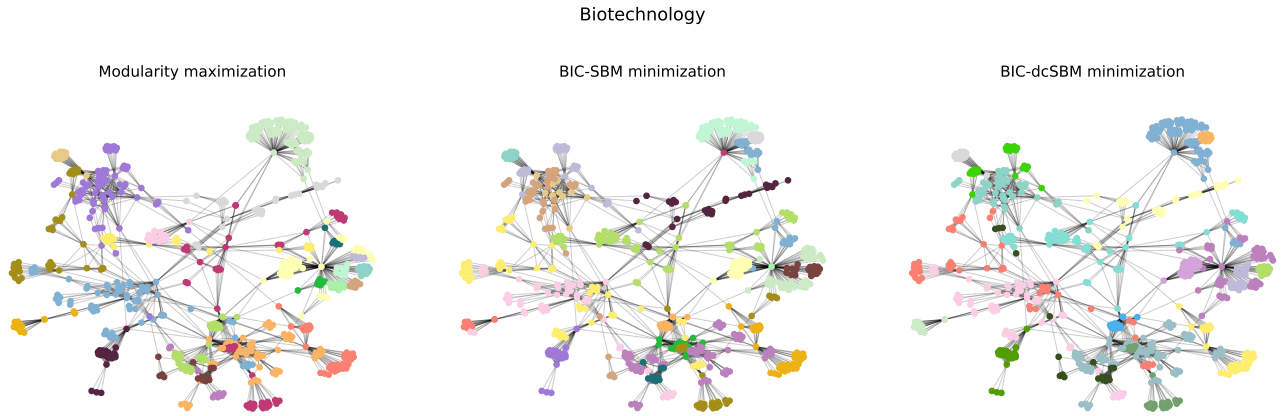


FIG. 8: **Mesoscale structure of the co-inventorship network in the biotech sector (top-700 actors).** The higher density and average clustering coefficient characterizing inventor networks reflect into a pronounced modular structure that points out field-specific specializations leading to project-based collaborations: this, in turn, suggests that knowledge recombines through phases of concentrated teamwork within communities.

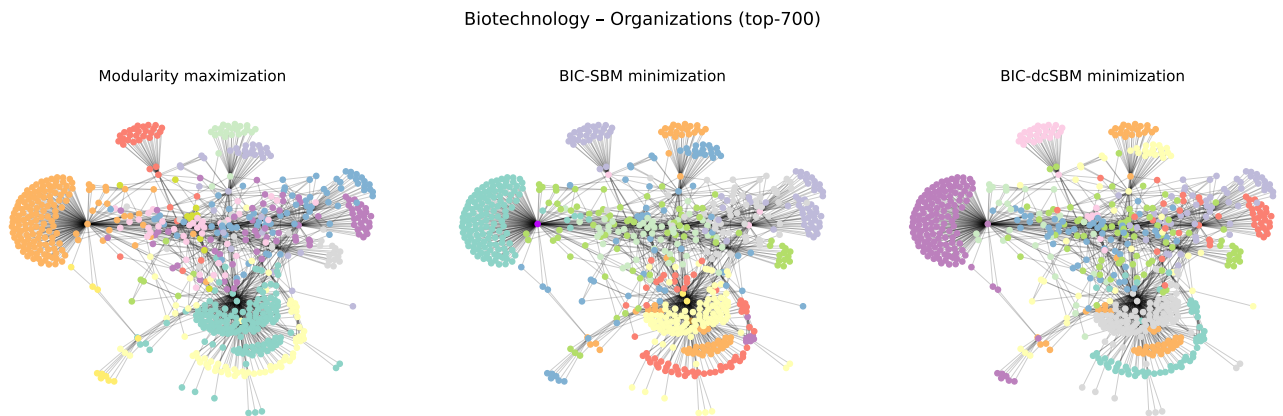


FIG. 9: **Mesoscale structure of the co-ownership network in the biotech sector (top-700 actors).** Differently from inventor networks, organization networks are much less modular, appearing as combinations of core-periphery structures: while few firms maintain many cross-institutional partnerships, most actors remain specialized or, at least, regionally confined; this, in turn, suggests that knowledge flows across communities in a hierarchical fashion.

Sector	Level	Top- <i>N</i>	Algorithm	# clusters	\bar{k}_{within}	σ_k^{within}	IC/EC	BIC-SBM	BIC-dcSBM	Q
AI	Inv.	300	Modularity maximization	10	19.14	17.14	3.81	13055.38	11163.24	0.5997
			BIC-SBM minimization	14	39.57	6.35	1.29	8572.59	-	0.4577
			BIC-dcSBM minimization	13	21.52	16.20	1.46	-	10040.69	0.4629
	700	700	Modularity maximization	17	12.78	16.35	3.61	35103.82	34159.62	0.6571
			BIC-SBM minimization	23	27.31	7.83	1.33	27060.18	-	0.4988
			BIC-dcSBM minimization	21	16.61	15.28	1.56	-	31075.17	0.5592
	Org.	300	Modularity maximization	11	4.23	6.98	3.18	5653.71	6630.15	0.6248
			BIC-SBM minimization	9	1.48	1.79	0.50	4376.08	-	0.2029
			BIC-dcSBM minimization	9	3.29	4.31	2.89	-	6525.58	0.6232
BT	Inv.	700	Modularity maximization	14	3.81	8.30	4.83	13871.12	17146.06	0.7160
			BIC-SBM minimization	13	17.82	4.57	0.90	11572.17	-	0.3807
			BIC-dcSBM minimization	12	4.13	8.29	3.94	-	17060.38	0.6973
	700	300	Modularity maximization	13	8.20	6.16	14.15	6734.43	8059.83	0.8220
			BIC-SBM minimization	15	10.60	4.51	3.58	5961.45	-	0.7104
			BIC-dcSBM minimization	14	9.07	5.80	7.45	-	7705.59	0.7977
	Org.	700	Modularity maximization	24	9.37	8.02	14.20	20116.88	23834.52	0.8538
			BIC-SBM minimization	24	19.09	4.76	5.31	17206.82	-	0.7836
			BIC-dcSBM minimization	20	10.85	7.67	11.44	-	22769.13	0.8506
SC	Inv.	300	Modularity maximization	9	4.18	12.59	4.02	5954.62	5741.52	0.5671
			BIC-SBM minimization	8	1.67	2.65	0.60	3220.73	-	0.2214
			BIC-dcSBM minimization	7	4.22	12.61	3.74	-	5672.67	0.5519
	700	300	Modularity maximization	13	4.33	12.25	3.78	15126.48	16645.30	0.6561
			BIC-SBM minimization	14	1.67	2.83	0.64	9795.19	-	0.3008
			BIC-dcSBM minimization	11	4.35	12.25	2.80	-	16248.27	0.6280
	Org.	700	Modularity maximization	10	8.99	9.23	6.13	9612.46	20906.33	0.6503
			BIC-SBM minimization	13	18.22	5.20	1.30	8408.14	-	0.4639
			BIC-dcSBM minimization	12	10.79	9.30	2.43	-	9939.78	0.6056
SC	Inv.	700	Modularity maximization	12	11.17	11.53	8.88	31407.89	50795.70	0.6987
			BIC-SBM minimization	22	16.05	7.67	1.31	27199.28	-	0.5013
			BIC-dcSBM minimization	21	14.05	11.23	2.13	-	31659.14	0.6078
	Org.	300	Modularity maximization	13	2.88	4.47	8.04	4483.67	6309.28	0.7646
			BIC-SBM minimization	9	11.03	2.71	1.37	3805.29	-	0.4484
			BIC-dcSBM minimization	7	3.24	4.48	9.38	-	6091.20	0.7473
	700	700	Modularity maximization	18	3.25	4.71	11.94	11678.41	17353.10	0.8409
			BIC-SBM minimization	14	9.71	3.66	4.54	10770.69	-	0.7349
			BIC-dcSBM minimization	13	3.66	4.73	9.88	-	16812.80	0.8279

TABLE V: **Clusters diversity across sectors, levels, algorithms and sizes.** For each sector, level, algorithm and size the table reports the number of detected clusters, the BIC instantiated with the SBM and the dcSBM (only the relevant one for the corresponding partition, both for the partition maximizing modularity), the modularity Q , the within-cluster average degree $\bar{k}_{\text{within}} = R^{-1} \sum_{r=1}^R \bar{k}_r$, the within-cluster degree standard deviation $\sigma_k^{\text{within}} = R^{-1} \sum_{r=1}^R \sigma_k^r$ and the ratio between the partition-specific numbers of intra-cluster and inter-cluster edges IC/EC.

Appendix C: Codes for the implementation of the BIC-based community detection schemes

The code operates on binary, undirected networks and implements a community detection framework resting upon the optimization of the Bayesian Information Criterion.

Our mesoscale detection scheme is based on outer iterations that repeatedly rerun Leiden starting from the last available partition. A first run of Leiden is performed starting from either singleton communities or a user-supplied initialization; the resulting partition is, then, used as initial condition for a new Leiden run that uses the same BIC-based score function. After each run, the BIC of the resulting partition is evaluated and compared with the best value observed until then. The procedure is repeated until the partition becomes stable - meaning that two, consecutive outer runs return the same assignment - or the maximum number of outer iterations is reached. The algorithm returns the partition that achieves the lowest BIC across all runs.

The Leiden implementation follows the standard, three-step structure, consisting of *i*) greedy node movement, *ii*) refinement and *iii*) aggregation. At the first step, nodes are visited in random order and moved to neighboring communities whenever this produces a positive gain in the quality score, i.e. a reduction of the BIC value. During the refinement step, each community from the previous iteration is further split by a local Leiden pass restricted to the nodes inside that community: this guarantees that each community in the refined partition is internally well-connected. At the aggregation step, communities are collapsed into supernodes and a coarse grained graph is built by summing the entries of the adjacency matrix over the corresponding node sets. The refined partition is lifted to

Algorithm 1: Leiden algorithm for the exploration of partitions

```

1: function Leiden(G, quality, initial)
2:   if an initial partition is provided then
3:     initialize each node to its community in the input partition
4:   else
5:     assign each node to its own singleton community
6:   end if
7:   prev  $\leftarrow$  None
8:   while True do
9:     randomly shuffle the nodes into a list Q
10:    while Q  $\neq \emptyset$  do
11:      pop first node v from Q
12:      let Cv be the community of v
13:      find communities of neighbors of v and add an empty community as candidate
14:      for each candidate community C' do
15:        compute  $\Delta Q$  = quality delta for moving v to C'
16:      end for
17:      choose a community C* that gives the maximum positive  $\Delta Q$  (if any)
18:      if  $\Delta Q > 0$  then
19:        move v to C*
20:        for each neighbor u of v that does not belong to C*, add u to Q (if not already present)
21:      end if
22:    end while
23:    if no node moved or all communities are singletons then
24:      return current community assignment as flat partition
25:    end if
26:    prev  $\leftarrow$  current partition
27:    start refinement step
28:    assign each node to its own singleton community in a refined partition
29:    for each community C in previous partition do
30:      let T be the set of nodes in C
31:      run a local Leiden pass on the induced subgraph on T, initialized from the current labels
32:      update the refined partition within T according to this local optimization
33:    end for
34:    aggregate nodes of the refined partition into supernodes
35:    build a new graph G' where each node is a refined community
36:    lift the refined partition to G' by assigning each supernode to a community label
37:    replace G with G' and continue
38:  end while
39: end function

```

this coarse graph, that becomes the input for the next iteration. The inner Leiden loop stops when no node moves or when a stopping criterion is reached.

Our framework exposes a single quality function interface, with specializations for the SBM or its degree-corrected variant. For what concerns the SBM, the probability of a link between nodes i and j depends only on their community labels. The model parameters are block-wise probabilities, estimated from the observed adjacency matrix and the candidate partition by counting the (missing) links between communities. The corresponding log-likelihood and BIC values are computed once per partition and used to define the quality score used by Leiden.

Algorithm 2: Community detection by minimizing BIC-SBM

```

1: function iterative_leiden_SBM( $G, \mathbf{A}, \dots$ )
2:    $qf \leftarrow \text{SBM\_BIC\_Quality}(\mathbf{A})$ 
3:    $\text{part} \leftarrow \text{Leiden}(G, qf, \text{initial} = \text{None})$ 
4:    $\text{best\_part} \leftarrow \text{part}$ ,  $\text{best\_bic} \leftarrow \text{BIC\_SBM}(\mathbf{A}, \text{part})$ 
5:   for  $i = 1 \dots \text{max\_outer}$  do
6:      $\text{new\_part} \leftarrow \text{Leiden}(G, qf, \text{initial} = \text{best\_part})$ 
7:     if  $\text{new\_part} = \text{best\_part}$  then break
8:      $\text{new\_bic} \leftarrow \text{BIC\_SBM}(\mathbf{A}, \text{new\_part})$ 
9:     if  $\text{new\_bic} < \text{best\_bic}$  then
10:        $\text{best\_part} \leftarrow \text{new\_part}$ ,  $\text{best\_bic} \leftarrow \text{new\_bic}$ 
11:     end if
12:   end for
13:   return  $\text{best\_part}, \text{best\_bic}$ 
14: end function

```

The dcSBM introduces node-specific degree parameters and block-specific affinity coefficients. Since a direct calculation of all parameters at every step would be computationally expensive and prone to convergence issues, our implementation follows a two-step approach. First, the UBCM is solved through a root finding routine: this provides an approximate set of degree parameters that is kept fixed throughout all outer Leiden iterations. Given these parameters, the code runs Leiden using a dcSBM-based quality score in which only the block affinities are adjusted. The outer loop described above is, then, applied exactly as for the SBM: each run of Leiden starts from the current best partition and the resulting BIC-dcSBM compared with the best value observed until then. After convergence of the outer loop, a final fit of the dcSBM is performed on the selected partition, by jointly updating the degree parameters and the block affinities. This last step is solely used to calculate the correct value of the BIC-dcSBM associated with the final partition - which is the value reported in the analysis.

The implementation is designed to be reproducible. All sources of randomness, including the random order in which nodes are visited and the initial partition when Leiden is seeded from random labels, are controlled by explicit seeds that can be passed to the high-level interface. Using the same seed, data, and hyperparameters produces the same sequence of partitions and the same BIC trajectory; at the same time, the code allows the user to initialize

Algorithm 3: Community detection by minimizing BIC-dcSBM

```

1: function iterative_leiden_dcSBM( $G, \mathbf{A}, \dots$ )
2:   estimate initial degree parameters  $\mathbf{x}$  by calling solve_UBCM_iterative on the observed degree sequence]
3:   define dcSBM BIC quality function  $qf$  using  $\mathbf{A}$  and fixed  $\mathbf{x}$ 
4:    $\text{part} \leftarrow \text{Leiden}(G, qf, \text{initial} = \text{None})$ 
5:    $\text{best\_part} \leftarrow \text{part}$ ,  $\text{best\_bic} \leftarrow \text{BIC\_dcSBM}(\mathbf{A}, \text{part}, \mathbf{x})$ 
6:   for  $i = 1 \dots \text{max\_outer}$  do
7:      $\text{new\_part} \leftarrow \text{Leiden}(G, qf, \text{initial} = \text{best\_part})$ 
8:     if  $\text{new\_part} = \text{best\_part}$  then break
9:      $\text{new\_bic} \leftarrow \text{BIC\_dcSBM}(\mathbf{A}, \text{new\_part}, \mathbf{x})$ 
10:    if  $\text{new\_bic} < \text{best\_bic}$  then
11:       $\text{best\_part} \leftarrow \text{new\_part}$ ,  $\text{best\_bic} \leftarrow \text{new\_bic}$ 
12:    end if
13:   end for
14:   compute block counts  $\mathbf{L}_{\text{obs}}$  from  $\text{best\_part}$ 
15:   obtain refined  $(\mathbf{x}_{\text{final}}, \boldsymbol{\chi}_{\text{final}})$  by calling solve_dcSBM_iterative on  $(\mathbf{k}, \text{best\_part}, \mathbf{L}_{\text{obs}}, \mathbf{x})$ 
16:    $\text{final\_bic} \leftarrow \text{BIC\_dcSBM}(\mathbf{A}, \text{best\_part}, \mathbf{x}_{\text{final}}, \boldsymbol{\chi}_{\text{final}})$ 
17:   return  $\text{best\_part}, \text{final\_bic}$ 
18: end function

```

Algorithm 4: Iterative resolution of the UBCM

```

1: function solve_UBCM_iterative(k, x0, ... )
2:   x  $\leftarrow$  x0, n  $\leftarrow$   $\|\text{residuals\_UBCM}(\mathbf{x}, \mathbf{k})\|$ 
3:   store (x, n) as current best solution, initialise patience counter]
4:   for i = 1 ... max_iter do
5:     x'  $\leftarrow$  root(residuals_UBCM, x)
6:     n'  $\leftarrow$   $\|\text{residuals\_UBCM}(\mathbf{x}', \mathbf{k})\|$ 
7:     if n' < n then
8:       update best solution to (x', n'), reset patience counter]
9:       x  $\leftarrow$  x', n  $\leftarrow$  n'
10:    else
11:      decrease patience counter]
12:    end if
13:    if n' < tol or patience counter expired then break
14:   end for
15:   return best pair (x, n)
16: end function

```

Algorithm 5: Iterative resolution of the dcSBM

```

1: function solve_dcSBM_iterative(k, c, Lobs, u0, ... )
2:   (pairs, idx)  $\leftarrow$  make_block_struct(c)
3:   define f( $\log \mathbf{u}$ ) = residuals_numba( $\log \mathbf{u}$ , k, c, Lobs, pairs, idx)
4:   initialise  $\log \mathbf{u} \leftarrow \log(\mathbf{u}_0)$ , and compute n  $\leftarrow \|f(\log \mathbf{u})\|$ 
5:   store ( $\log \mathbf{u}$ , n) as current best solution, initialise patience counter]
6:   for i = 1 ... max_iter do
7:     compute an updated vector  $\log \mathbf{u}'$  using a nonlinear solver applied to f
8:     n'  $\leftarrow \|f(\log \mathbf{u}')\|$ 
9:     if n' < n then
10:       update best solution to ( $\log \mathbf{u}'$ , n'), reset patience counter]
11:        $\log \mathbf{u} \leftarrow \log \mathbf{u}'$ , n  $\leftarrow$  n'
12:     else
13:       decrease patience counter]
14:     end if
15:     if n' < tol or patience counter expired then break
16:   end for
17:   return ( $\exp(\log \mathbf{u}_{\text{best}})$ , nbest)
18: end function

```

Leiden with a user-supplied partition, a modularity-based partition, or with the partition constituted by singletons. When a modularity-based initialization is used, an external modularity-maximization routine is run once to obtain a starting partition: this partition is, then, refined by the BIC-based outer iterations; when the partition constituted by singletons is used, each node starts as a community on its own and the method refines such an assignment from scratch.

Appendix D: Robustness checks

To test the robustness of our results, we have replicated our analysis on the representations of our system induced by the top-300 and top-700 most connected nodes and compared them with the one carried out on the main sample. As fig. 10, across all sectors and levels, the complementary cumulative degree distributions (CCDFs) preserve their heavy-tailed shape, with only minor shifts in slope due to the sample size. Inventor networks are less heterogeneous and more clustered than organization networks, thus confirming that cohesive small-team structures coexist with few, highly-connected nodes. Besides, expanding from 300 to 700 nodes does not alter the relative patterns among sectors: AI and BT remain the most clustered, while SC exhibits more even degrees and a lower cohesion. Overall, thus, the main findings are not affected by the selection of the top actors.

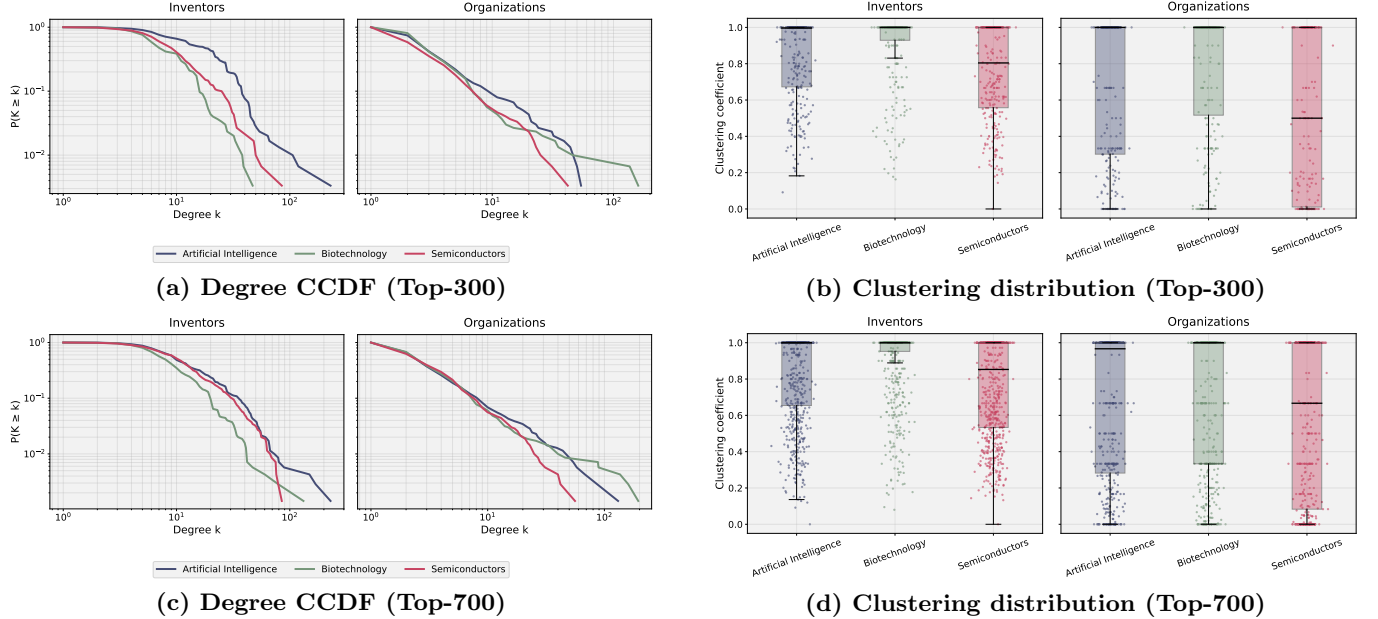


FIG. 10: **Robustness checks across network sizes.** Left column: complementary cumulative degree distributions and clustering coefficient distributions for inventor and organization networks in the three, strategic sectors of artificial intelligence, biotechnology and semiconductors (left column: only the top-300 actors have been considered; right column: only the top-700 actors have been considered). Across all sectors and levels, the patterns are consistent with the ones shown in the main text.

To assess the similarity between partitions, we have computed the *Rand Index* (RI), the *Jaccard Index* (JI) and the *Normalized Mutual Information* (NMI) [64]. The RI [65] measures the percentage of node pairs that are grouped together and separated in both partitions. The Jaccard index [66] solely focuses on the pairs of nodes that belong to the same cluster in both partitions. The NMI [67] quantifies the amount of shared information between the two partitions. Each index ranges between 0 and 1, with 0 indicating maximum difference and 1 indicating perfect similarity.

In standard settings, these indices are used to compare a ‘test partition’ against a ‘ground-truth’ one. Here, however, no ground-truth is available and the indices are employed to compare any two partitions (say, C and D) obtained from different algorithms. This naturally raises the question of whether the indices depend on the order in which the two partitions are compared. To clarify this point, it is useful to rewrite the definitions of the indices above in terms of the classical contingency counts between C and D . Let *i*) TP denote the number of node pairs placed together in both partitions, *ii*) TN the number of node pairs separated in both, *iii*) FP the number of node pairs that are placed together in D but separated C , *iv*) FN the number of node pairs that are put together in C but separated D . The Rand Index, then, reads

$$RI(C, D) = \frac{TP + TN}{TP + TN + FP + FN}, \quad (D1)$$

the Jaccard Index, then, reads

$$JI(C, D) = \frac{TP}{TP + FP + FN} \quad (D2)$$

and the Normalized Mutual Information, then, reads

$$NMI(C, D) = \frac{2MI(C, D)}{H(C) + H(D)}, \quad (D3)$$

where $MI(C, D) = \sum_{i=1}^N \sum_{j=1}^N h_{ij} \ln(h_{ij}/f_i g_j)$, with $H(C) = -\sum_{i=1}^N f_i \ln f_i$ and $H(D) = -\sum_{j=1}^N g_j \ln g_j$. Here, $h_{ij} = n_{ij}/N$ is the (joint) probability that a randomly chosen node belongs to community i in C and to community j in D , with n_{ij} being the size of the intersection between these two communities and N being the total number of nodes; correspondingly, $f_i = n_i/N$ and $g_j = n_j/N$ are the marginal probabilities that the same node belongs to community i in C and to community j in D , with n_i and n_j denoting their sizes [64]. All indices are symmetric: for what concerns the RI and the JI, exchanging the roles of C and D simply swaps the roles of FP and FN ; for what concerns the NMI, symmetry follows from noticing that $MI(C, D) = MI(D, C)$ and $H(C) + H(D) = H(D) + H(C)$.

Table VI reports the similarity scores between the partitions retrieved by our algorithms: *i*) the similarity between partitions is consistently higher at the individual level than at the organization level. Inventor networks typically exhibit RI values above 0.93 and JI values in the range [0.45, 0.65], whereas organization networks frequently display lower agreement, with JI values often between 0.29 and 0.54. This confirms that inventor networks possess a more cohesive mesoscale structure, recognized by each algorithm, while organization networks are comparatively more diffuse, hence described differently by different algorithms; *ii*) according to the JI values, the partitions obtained by minimizing the BIC-dcSBM are, overall, more similar to those returned by modularity maximization than to those obtained by minimizing the BIC-SBM. This pattern indicates that accounting for degree heterogeneity mitigates the tendency of the BIC-SBM to ‘favor’ core-periphery structures - more specifically, to split the core-nodes and the peripheral ones, a tendency punished by the JI, that is sensitive to the number of false negatives (i.e. pairs of nodes grouped together in the first partition but separated in the second); *iii*) according to the NMI values, the partitions induced by minimizing the BIC-SBM and those obtained by minimizing the BIC-dcSBM are the most similar ones.

Sector	Level	Top- N	dcSBM vs SBM			dcSBM vs Q			SBM vs Q		
			NMI	RI	JI	NMI	RI	JI	NMI	RI	JI
AI	Inventors	300	0.830	0.951	0.560	0.745	0.900	0.413	0.774	0.909	0.472
		500	0.871	0.966	0.613	0.888	0.958	0.587	0.843	0.948	0.519
		700	0.824	0.967	0.497	0.769	0.938	0.388	0.761	0.933	0.368
	Organizations	300	0.629	0.869	0.375	0.813	0.932	0.525	0.662	0.875	0.378
		500	0.769	0.923	0.531	0.794	0.923	0.536	0.786	0.918	0.540
		700	0.622	0.889	0.302	0.812	0.954	0.615	0.633	0.886	0.291
BT	Inventors	300	0.880	0.960	0.586	0.909	0.967	0.683	0.826	0.936	0.461
		500	0.863	0.964	0.564	0.872	0.960	0.555	0.862	0.956	0.549
		700	0.897	0.975	0.652	0.857	0.960	0.528	0.822	0.951	0.424
	Organizations	300	0.734	0.895	0.592	0.709	0.907	0.618	0.635	0.871	0.511
		500	0.650	0.910	0.500	0.744	0.932	0.593	0.707	0.914	0.544
		700	0.719	0.937	0.566	0.710	0.919	0.500	0.647	0.906	0.458
SC	Inventors	300	0.712	0.914	0.384	0.795	0.903	0.444	0.739	0.887	0.407
		500	0.797	0.950	0.505	0.794	0.935	0.499	0.746	0.916	0.397
		700	0.771	0.946	0.382	0.734	0.901	0.348	0.709	0.892	0.291
	Organizations	300	0.735	0.906	0.534	0.810	0.928	0.546	0.761	0.906	0.469
		500	0.778	0.914	0.433	0.771	0.933	0.441	0.802	0.924	0.453
		700	0.817	0.943	0.505	0.787	0.938	0.423	0.798	0.943	0.483

TABLE VI: **Agreement between partitions across sectors, levels, algorithms and sizes.** For each sector, level, algorithm and size the table reports the Normalized Mutual Information (NMI), the Rand index (RI) and the Jaccard index (JI) between pairs of partitions. Across all settings, NMI and RI are typically larger than 0.70 while JI lies in the range [0.30, 0.70].

Finally, we have repeated the calculation of the Lorenz curves. As fig. 11 shows, the overall patterns closely match the ones shown in the main text: *i*) a limited subset of communities concentrates a large share of forward citations; *ii*) inventor networks are more unequal than organization networks. These patterns are fully consistent with the Gini coefficients reported in table VII.

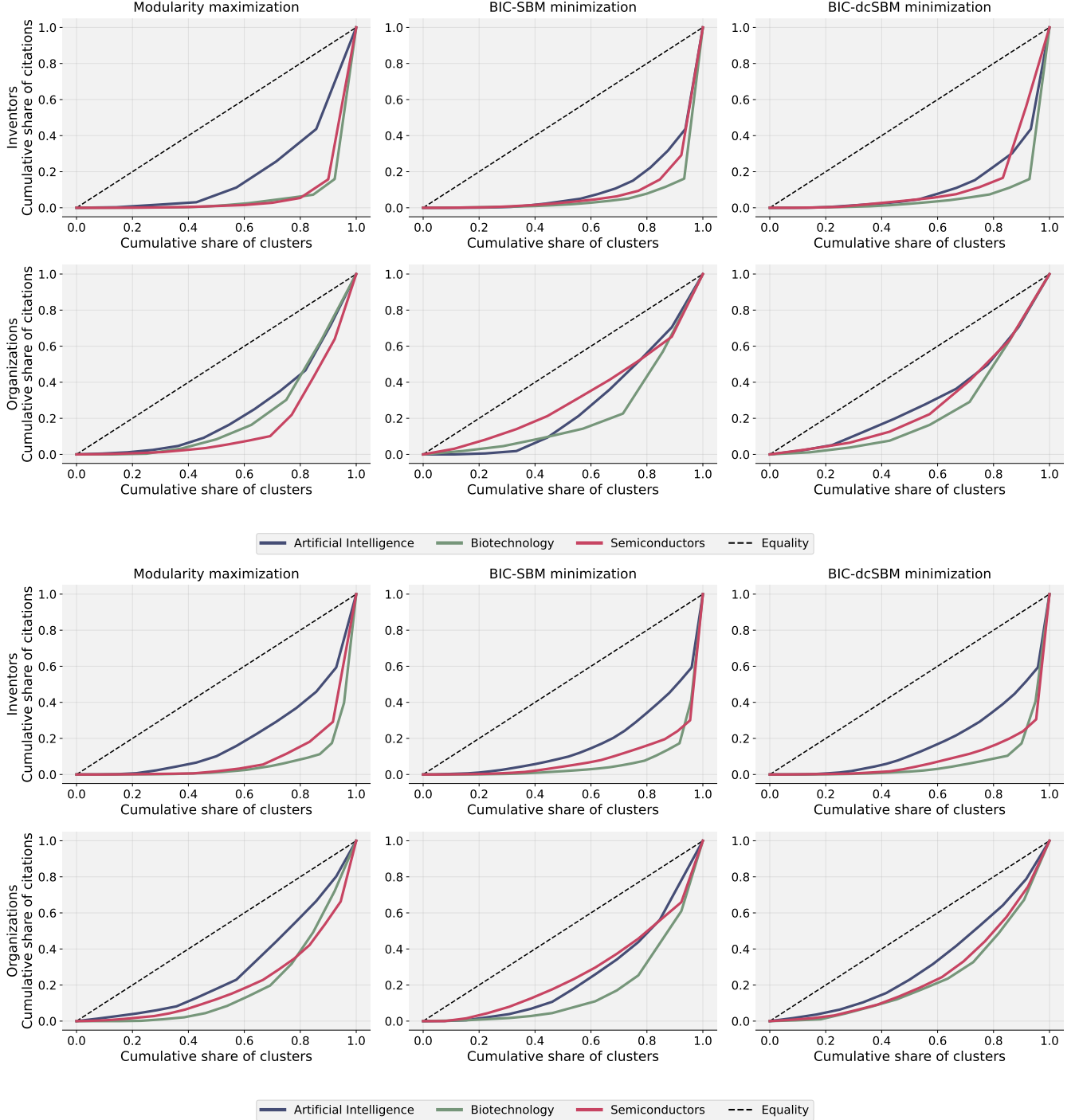


FIG. 11: **Inequality of the innovation impact across sizes.** Lorenz curves of forward citations for inventor and organization networks (top panels: only the top-300 actors have been considered; bottom panels: only the top-700 actors have been considered). Inequality patterns are consistent with the ones shown in the main text: inventor networks show a steadily high inequality across sectors, whereas organization networks are more diverse, with the AI sector exhibiting the highest level of inequality.

Top- N	Level	Sector	Gini on Q	Gini on BIC-SBM	Gini on BIC-dcSBM
300	Inventors	AI	0.612	0.758	0.741
		BT	0.864	0.862	0.853
		SC	0.846	0.810	0.739
	Organizations	AI	0.522	0.462	0.392
		BT	0.570	0.544	0.511
		SC	0.677	0.362	0.432
500	Inventors	AI	0.826	0.811	0.826
		BT	0.841	0.865	0.845
		SC	0.803	0.817	0.840
	Organizations	AI	0.659	0.686	0.590
		BT	0.353	0.574	0.441
		SC	0.570	0.367	0.278
700	Inventors	AI	0.594	0.645	0.635
		BT	0.862	0.858	0.846
		SC	0.799	0.808	0.807
	Organizations	AI	0.420	0.492	0.367
		BT	0.611	0.652	0.517
		SC	0.587	0.459	0.481

TABLE VII: **Inequality of innovation impact across sectors, levels, algorithms and sizes.** For each sector, level, algorithm and size the table reports the Gini coefficient of the distribution of citations across the mesoscale structures of inventor and organization networks. Higher values indicate more unequal distributions (equivalently, concentrations) of citations across clusters.